

GTC Spectra of $z \approx 2.3$ Quasars: Comparison with Local Luminosity Analogues

Jack W. Sulentic¹, Paola Marziani², Ascensión del Olmo¹, Deborah Dultzin³, Jaime Perea¹, and C. Alenka Negrete⁴

¹ Instituto de Astrofísica de Andalucía, IAA-CSIC, Glorieta de la Astronomía s/n 18008 Granada, Spain. e-mail: sulentnic@iaa.es, chony@iaa.es, jaime@iaa.es

² INAF, Osservatorio Astronomico di Padova, vicolo dell' Osservatorio 5, IT 35122, Padova, Italy. e-mail: paola.marziani@oapd.inaf.it

³ Instituto de Astronomía, Universidad Nacional Autónoma de México, Mexico D.F. 04510, Mexico e-mail: deborah@astro.unam.mx

⁴ Instituto Nacional de Astrofísica, Óptica y Electrónica, Tonantzintla, Puebla, Mexico. e-mail: cnegrete@inaoep.mx

ABSTRACT

Context. The advent of 8-10m class telescopes makes possible for the first time detailed comparison of quasars with similar luminosity and very different redshifts.

Aims. A search for z -dependent gradients in line emission diagnostics and derived physical properties by comparing, in a narrow bolometric luminosity range ($\log L \sim 46.1 \pm 0.4$ [erg s⁻¹]), some of the most luminous local $z < 0.6$ quasars with some of the lowest luminosity sources yet found at redshift $z = 2.1 - 2.5$.

Methods. Moderate S/N spectra for 22 high redshift sources were obtained with the 10.4m Gran Telescopio Canarias (GTC) while the HST (largely Faint Object Spectrograph) archive provides a low redshift control sample. Comparison is made in the context of the 4D Eigenvector 1 formalism meaning that we divide both source samples into high accreting Population A and low accreting Population B sources.

Results. C $\nu\lambda 1549$, the strongest and most reliable diagnostic line, shows very similar properties at both redshifts confirming at high redshift the C $\nu\lambda 1549$ profile differences between Pop. A and B that are well established in local quasars. The C $\nu\lambda 1549$ blueshift that appears quasi-ubiquitous in higher L sources is found in only half (Population A) of quasars observed in both of our samples. A C $\nu\lambda 1549$ evolutionary Baldwin effect is certainly disfavored. We find evidence for lower metallicity in the GTC sample that may point toward a gradient with z . No evidence for a gradient in M_{BH} or L/L_{Edd} is found.

Conclusions. Spectroscopic differences established at low z are also present in much higher redshift quasars. Our results on the C $\nu\lambda 1549$ blueshift suggest that it depends on both source luminosity and L/L_{Edd} . Given that our samples involve sources with very similar luminosity the evidence for a systematic Z decrease, if real, points toward an evolutionary effect. Our samples are not large enough to effectively constrain possible changes of M_{BH} or L/L_{Edd} with redshift. Both samples appear representative of a slow evolving quasar population likely present at all redshifts.

Key words. quasars: emission lines – quasars: supermassive black holes – ISM: abundances – line: profiles – cosmology: observations

1. Introduction

It has been known for decades that quasars show evolution with redshift (Schmidt 1968; Schmidt & Green 1983). The brightest quasars at redshifts $z \gg 1.0$ are much more luminous than any local quasars (often called Seyfert 1s if they show a host galaxy). Locally ($z \lesssim 0.5$) we find quasars with absolute magnitudes in the range $M_B = -23$ to -25 (we ignore here AGN below -23 which was a kind of historical boundary between type-1 quasars and Seyfert 1 galaxies). At redshift $z \approx 2.3$ (the quasar number density peaks near there: Schmidt et al. 1995; Boyle et al. 2000) we find sources in the range $M_B = -25$ to -29 while sources in this luminosity range are almost nonexistent locally. At redshift $z \approx 4$ we observe $M_B = -27$ to -30 superluminous quasars that are 2dex more luminous than any local sources.

We are forced to conclude that the most luminous quasars show strong evolution in their space density. In fact they no longer exist. Does this mean that all quasars show evolution or is it purely luminosity driven? Figure 1 illustrates the observational situation by plotting the distribution of a representative

SDSS quasar subsample (Schneider et al. 2010) in the $z - B$ absolute magnitude plane. Note that only sources listed as quasars in the Schneider et al. (2010) catalogues are shown so that a large population of local AGN (Koehler et al. 1997) and AGN with the narrowest (FWHM < 1000 km s⁻¹) broad lines (Zhou et al. 2006) are not shown in the lower part of the plot. The low- z yellow box identifies a range of absolute magnitudes where quasars are rare in the local Universe (they would be easily detected, but they do not exist in large numbers) and belong to the high luminosity tail of the optical luminosity function (Cheng et al. 1985; Grazian et al. 2000; Richards et al. 2005). If analogues to local quasars exist at all redshifts then the lower right quadrant of the plot will be well populated when they are found. They would be generally fainter than $m_B \approx 22$ and until very recently were not easy to find; however, that situation is changing rapidly thanks to SDSS-III/BOSS (Ahn et al. 2014).

Historical attempts to compare quasars with similar luminosity at significantly different redshifts were few and difficult. We have more often compared the brightest quasars at different redshifts because it has been almost impossible to obtain good spec-

tra for fainter sources (luminosity analogues of low z sources) using 2–4m class telescopes. This means that we are usually comparing quasars in very different optical luminosity ranges. This limitation is quite relevant if optical luminosity plays an important role in quasar evolution and obscures other physical drivers. We are unable to search effectively for signatures of luminosity-independent evolution (e.g. metallicity, BLR structure/geometry geometry, M_{BH} and accretion rate). Spectroscopy provides the most powerful clues about most of these things. Obtaining spectra for $z \geq 2.0 - 2.5$ luminosity analogues of nearby quasars involves spectroscopy of faint sources $m_{\text{B}} = 21 - 23$. It is one thing to obtain spectra in order to confirm the existence of faint quasars and quite another to obtain spectra with s/n and resolution permitting more detailed studies.

There is a growing consensus that the leading parameter governing quasar diversity involves the Eddington ratio (e.g., Marziani et al. 2001; Baskin & Laor 2004; Dong et al. 2009; Brightman et al. 2013). Other factors likely play important roles and have been discussed in recent review papers (e.g., Marziani et al. 2006; Marziani & Sulentic 2013). We note that a key complication affecting the quasars (and not stars) is that our measures are affected by line-of-sight orientation (Sulentic et al. 2003; Collin et al. 2006; Boroson 2011; Runnoe et al. 2013). Metallicity effects also significantly affect the observed spectra of quasars (e.g., Ferland et al. 1996; Shemmer et al. 2004; Netzer & Trakhtenbrot 2007).

One might ask if high redshift analogues of local low luminosity quasars even exist? Perhaps all quasars were luminous “monsters” at high redshift and we are witnessing a systematic downgrading of activity with increasing cosmic time. In this view the youngest quasars at any epoch grow so fast that we observe very few in the process of rapid accretion. The currently favored view is that rapidly accreting “monster” quasars exist side-by-side with slower growing quasars (AGN) and that the latter exist at all redshifts (Trakhtenbrot et al. 2011). The monsters have gradually disappeared and are no longer seen below $z \approx 2.0$. The slower evolving quasar population is assumed to be plentiful, perhaps even more numerous than at low redshift? Is the peak in quasar density near $z \approx 2.3$ (e.g., Fan 2006) driven largely or totally by the luminous population that has ceased to exist? Do high redshift analogues of local quasars show the same space density at all redshifts as well as the same emission line properties, black holes masses and Eddington ratios? The few studies of low L quasars at high z so far have focussed on estimating the space density of these sources (Glikman et al. 2011; Ikeda et al. 2012). We focus instead on trying to answer some of the questions raised above. The fainter, assumed slower evolving, quasars of interest in this study are largely absent above $z \sim 1$ in Figure 1 because they were not spectroscopically sampled by SDSS. Up to the present they have more often been discovered in deep radio, X-ray or optical pencil beam surveys. At redshifts above $z \sim 1$, SDSS I/II surveyed quasars largely brighter than $m_{\text{B}} \approx 20 - 21$. If high redshift analogues of low luminosity/redshift quasars exist in abundance are they spectroscopically different in any way? This question motivated our study.

One of the many technological changes that has taken place over the 50 years since the discovery of quasars involves the advent of 8–10m class telescopes equipped with CCD imaging spectrographs. We are now entering the era when we can effectively compare quasars of very similar luminosity at very different redshifts. We report here on a pilot survey of $z \approx 2.1 - 2.4$ quasars with luminosities in the range $M_{\text{B}} = -23$ to -25 which is the same range as low luminosity quasars found at

low z (down to the most luminous local Seyfert galaxies). Section 2 describes the survey, source sample, low- z control sample and reduction procedures. Section 3 presents the high- z source spectra and emission line parameters derived from them. Section 3.2 presents a comparison of mean/median properties for the high and low- z samples. This is followed by comparison in the 4D Eigenvector (4DE1) context where we distinguish and compare Population A and B sources separately. Section 4 discusses implication of our findings in terms of quasar evolution, focusing on observational parameters, gas metallicity, black hole mass and Eddington ratio. Finally we present in Appendix A the analysis of a red quasar that showed up in our sample.

2. Spectroscopic Samples and Reductions

2.1. Sample Selection Strategy

The goal of the present study was to make a spectroscopic survey of quasars in the range $z = 2.1 - 2.5$ with luminosities similar to local sources. We required high enough s/n to allow detailed comparison with properties of a low redshift control sample taken from the HST archive. This was a pencil-beam survey in the sense that the same spectral region ($\text{Ly}\alpha\text{-CIV}]1909$) was sampled over a very narrow z , M_{B} range. The z range was chosen to be as high as possible in order to sample quasars at a cosmologically significant epoch. The M_{B} range involved luminosities as low as possible (just above the nominal Seyfert 1 – type 1 quasar boundary at $M_{\text{B}} = -23.0$). We would have preferred to go 1–2 magnitudes fainter but the adopted range was dictated by available telescope time and instrumentation. This translates to sources in the apparent magnitude range $m_{\text{B}} \sim 20.0 - 22.0$ which corresponds to $M_{\text{B}} \approx -23$ to -25 (and bolometric luminosity $\log L \sim 45.7 - 46.5$).

Steps to find low luminosity quasars at $z \approx 2.5$ involved a search for faint previously identified quasars in the Véron-Cetty & Véron catalog (e.g., Véron-Cetty & Véron 2010): since we did not carry out a new quasar survey. Many of our adopted targets are SDSS sources, but lacked spectroscopic follow-up in either SDSS-I/II or SDSS-III/BOSS at the time of our survey. Sources were selected in narrow redshift ($2.3 \lesssim z \lesssim 2.5$) and absolute magnitude ($-25 \lesssim M_{\text{B}} \lesssim -23$) ranges. The high and low z regions of interest are marked in (Fig. 1). More than 2700 candidate sources are found in the 13th edition of Véron-Cetty & Véron (2010). Clearly the number of low/intermediate luminosity quasars at high z is increasing rapidly. Targets were selected randomly and are listed in Table 1 which presents quasar identification, apparent magnitude, redshift $\pm 1\sigma$ uncertainty (see §2.3), absolute B magnitude from Véron-Cetty & Véron (2010), discovery technique or detection band, a reference to the discovery paper, an alternate name and some additional information notably on radio flux for radio detected sources. As expected many chosen sources have names reflecting discovery in X-ray surveys or deep optical searches (Table 1, columns 7–8). The flux limits associated with optical surveys cause an “Eddington ratio bias” as shown in Figure 2. Fig. 2 gives a graphical representation for the case of a typical ($10^8 M_{\odot}$) and a large black hole mass ($10^{9.5} M_{\odot}$). Bands of different colors identify sources radiating in different Eddington ranges. Sources radiating close to or somewhat below the Eddington limit are indicated as NLSy1-like quasars (Pop. A in 4DE1 parlance, Sulentic et al. 2000b; Netzer 2013 and §4). Below $L/L_{\text{Edd}} \approx 0.2$ we find no change in observational properties (Pop. B; Sulentic et al. 2008, 2011), while below $L/L_{\text{Edd}} \approx 0.01$ accretion processes may become unstable and the quasar state

may be transient. The flux limit associated with a survey introduces a bias in the discovery of quasars: in the example of Fig. 2 all quasars at $z \lesssim 0.3$ with $M_{\text{BH}}=10^8 M_{\odot}$ can be detected while at $z \approx 2.3$ only quasars radiating close to the Eddington limit will be detected within a limiting magnitude $m_B \approx 21.5$. Only quasars with the largest masses will be detected at $z \approx 2.3$. This mass-dependent loss of low Eddington ratio sources will be a source of bias at high z .

2.2. Observations and Data Reduction

Using the 10m GTC equipped with the faint-object spectrograph OSIRIS it is possible to obtain $S/N \approx 20$ spectra of quasars in the $m_B \approx 21 - 22$ magnitude range with exposures of about 40 minutes in good seeing. Under less than optimal conditions we will obtain spectra with $S/N \approx 7 - 12$. Within the observed wavelength range we obtain several lines (from $\text{Ly}\alpha$ to $\text{CIII}\lambda 1909$) from which diagnostics intensity ratios can be computed. The GTC spectra are similar to or better than the HST archival UV spectra for low redshift analogues (Bachev et al. 2004; Sulentic et al. 2007). Figure 3 shows a montage of the deredshifted GTC spectra obtained for 22 quasars. One source (Wee 155) turned out to have an incorrect redshift ($z \approx 1.59$) derived from the low S/N discovery spectrum. An additional source is obviously a heavily reddened (radio-loud if no correction for extinction is applied) quasar FIRST J15318+2423. (discussed in Appendix A). The remaining 20 sources represent our working sample of unreddened low luminosity quasars (2 radio-loud). Spectra show S/N near 10 – 20 covering $\text{Ly}\alpha - \text{CIII}\lambda 1909$ in the rest frame. They can be effectively compared with low z UV spectra from the HST archive already studied in the 4DE1 context (Bachev et al. 2004; Sulentic et al. 2007). Our high z sample clusters near $\log L_{\text{bol}} \sim 46.0$ with redshift range from $z = 2.21 - 2.40$.

Long slit spectroscopic observations of the selected quasars were carried out with OSIRIS (Optical System for Imaging and low-Intermediate-Resolution Integrated Spectroscopy) located at the Nasmyth-B focus of the 10.4m GTC telescope of the Observatorio del Roque de los Muchachos (La Palma, Spain). The observations were obtained in service mode in two approved observing programs during 2011 and 2013. In the first run 15 QSOs were observed while 7 more were obtained during the spring 2013 run. The R1000B grism was used for all observations with 2×2 binning yielding a wavelength range of 3650 – 7750 Å with a reciprocal dispersion of about 2.1 Å/pixel ($R = \lambda/\delta\lambda \approx 1000$). This coverage corresponds to the wavelength region of interest for our study from $\text{Ly}\alpha$ to $\text{CIII}\lambda 1909$ and includes $\text{NV}\lambda 1240$, $\text{SiIV}\lambda 1397$ & $\text{OIV}\lambda 1402$, $\text{CIV}\lambda 1549$, $\text{AlIII}\lambda 1860$ or $\text{SiIII}\lambda 1892$ emission lines. The slit was oriented at parallactic angle to minimize effects of atmospheric differential refraction in the spectra. Table 2 gives a log of the observations where columns list in this order: QSO ID, date of observation, total exposure time in seconds, the number of split exposures, the signal/noise measured in the combined spectrum for each object (at 1450 Å; blueward of the $\text{CIV}\lambda 1549$ line), the slit width in arcsec, and the seeing measured by fitting several stars in the acquisition image of each quasar.

Data reduction was carried out in a standard way using the IRAF package. The task CCDPROC was used to trim the spectra and make the overscan correction. Bias subtraction was performed nightly by subtracting a median zero-level bias image constructed by combining all bias frames provide by the telescope team. Also each spectrum was flat-field corrected with

the normalized flat-field obtained after median combination of the flats obtained with the same instrumental setup. 2D wavelength calibration was obtained using the combination of HgAr and Ne lamp exposures and IRAF routines IDENTIFY, REIDENTIFY, FITCOORDS, and TRANSFORM. We checked wavelength calibration for all the individual exposures of each objects before final combination. The APALL task was used for object extraction and background subtraction. Instrumental response and flux calibration were obtained from spectrophotometric standard star exposures with the same instrumental configuration, provided for each night our sources were observed (Ross 640, Feige 34, GD 24, GRW+70.8247 and Feige 92 [for the first run]; Feige92, Ross 640, G157-32 and GD 140 [for the second run]).

2.3. Data Analysis

Spectra were reduced to rest frame wavelength and specific flux scale. An unbiased estimate of the redshift (i.e. source rest frame) is not trivial because the GTC spectra only cover the UV domain where narrow low ionization lines (LILs), usually the most reliable rest frame indicators (Eracleous & Halpern 2003; Hu et al. 2008) are not available. We therefore estimated redshifts from low-ionization $\text{OII}\lambda 1304$, $\text{SiII}\lambda 1264$, $\text{CII}\lambda 1334$ features as well as $\text{CIII}\lambda 1909$, including $\text{CIV}\lambda 1549$ and other high ionization lines only if they showed values consistent with the LILs. Uncertainties are reported in Table 1 with the rest frame estimated to be accurate to $\pm 200 \text{ km s}^{-1}$ for most sources ($\pm 300 \text{ km s}^{-1}$ for three sources). The LIL features were not measured in one source ([VCV96] 1721.4+3401) so the redshift rests on $\text{CIV}\lambda 1549$, $\text{Ly}\alpha$, and $\text{SiIII}\lambda 1892$. The first two lines yield a significantly lower value than $\text{SiIII}\lambda 1892$ leading to an estimated uncertainty of $\pm 500 \text{ km s}^{-1}$.

One of the first steps after data reduction was an attempt to separate sources into Population A and B following the 4DE1 formalism. Both optical and UV (as well as X-ray) criteria are summarized in Sulentic et al. (2007). Criteria employed in the present paper are also discussed in Negrete et al. (2014) and entail: (1) line widths of $\text{AlIII}\lambda 1860$ and $\text{SiIII}\lambda 1814$ are found to be correlated with $\text{H}\beta$ line width (Negrete et al. 2013a,b) making them useful Pop. A-B discriminators and virial estimators; (2) EW $\text{CIV}\lambda 1549$ values for Pop. A1 and B sources are a factor of two higher than for the rest of Pop. A sources and (3) blue and red $\text{CIV}\lambda 1549$ profile asymmetries appear to be signatures of Pop. A and B sources, respectively. The criteria allow a reasonable population A-B discrimination. Those near the intersection (bin A1) are much less certain and the bin is likely a mix of A and B sources. The fact that we find an even division between source populations (11 Pop. A and 9 Pop. B), as has been found at low redshift (Zamfir et al. 2010), suggests that our sample is a reasonably random selection of quasars in the context of 4DE1 (in (Zamfir et al. 2010) the magnitude limited SDSS sample divides 45% and 55% for pop. A and B respectively).

Intensity and profile measures of emission lines was carried out following the approach described in Marziani et al. (2010) and Negrete et al. (2013a). The salient assumption is that each line in a Pop A source can be interpreted as a composite of: an unshifted symmetric component plus a blueshifted, asymmetric component (BLUE) related to systematic outflow motions. In the case of Pop. B sources any blueshifted component is much weaker however a very broad and redshifted component (VBC) is usually seen along with the unshifted component that is assumed to arise in a virialized medium (the “classical” broad component; BC). These line components (BLUE, BC and VBC) were included when modelling the strongest emis-

sion lines $\text{Ly}\alpha$, $\text{Nv}\lambda 1240$, $\text{Civ}\lambda 1549$, $\text{HeII}\lambda 1640$, $\text{AlIII}\lambda 1860$, $\text{SiIII}\lambda 1892$, and $\text{CIII}\lambda 1909$. They were simultaneously fit along with continuum and $\text{FeII} + \text{FeIII}$ emission (the latter relevant only in the 1900 blend and for Pop. A only). In the case of the UV FeII and FeIII emissions we considered the templates provided by Brühweiler & Verner (2008) and Vestergaard & Wilkes (2001), respectively. The fitting routine scaled and broadened the original templates to reproduce the observed emission. FeII is always set to zero by the fitting routine reflecting its low intensity and the low S/N in the observed spectral range. The S/N of some spectra allow only a marginal fit with the greatest uncertainty involving the 1900 blend and the blue component in Pop B sources.

The 1900 blend has become important for several reasons: 1) FWHM $\text{AlIII}\lambda 1860$ and $\text{SiIII}\lambda 1892$ can be used as a virial estimator (Negrete et al. 2013a), and their FWHM can also be used for distinguishing Pop. A and B sources; 2) the relative strength of $\text{AlIII}\lambda 1860$, $\text{SiIII}\lambda 1892$, and $\text{CIII}\lambda 1909$ can be used as additional diagnostics for distinguishing between Pop. A and B quasars (Bachev et al. 2004; Negrete et al. 2013a), 3) line ratios involving $\text{SiIII}\lambda 1892/\text{Civ}\lambda 1549$ and $\text{AlIII}\lambda 1860/\text{SiIII}\lambda 1892$ are important for constraining BLR physical conditions that can be used to estimate the BLR radius (Negrete et al. 2013a). The key is to use spectra with S/N high enough to allow modelling and decomposition of the lines in the blend.

Figures 3, 4 and 5 show deredshifted spectra and individual fits for our GTC sample where S/N varies from 5 – 6 to 40. It is easy to see how the blend modelling becomes less certain for the lowest S/N examples.

2.4. A low redshift comparison sample of luminosity analogues

The significance of observations for high z low luminosity quasars can be fully understood only if a suitable low- z control sample exists for the same luminosity range. Archived HST/FOS observations provide spectra with similar dispersion, S/N and luminosity. The archival spectra were previously studied in the 4DE1 context (Bachev et al. 2004; Sulentic et al. 2007). The heterogeneous nature of both the GTC/OSIRIS and HST/FOS samples means that neither is complete.

The FOS sample in particular is strongly biased towards radio loud sources. We randomly extracted smaller subsamples satisfying the conditions: (1) absolute magnitude distribution not statistically different from the GTC sample; (2) consistent fraction of radio sources ($\approx 10\%$ as in the GTC sample). In practice sources were selected from the sample of 130 sources given in Tables 1 and 2 of Sulentic et al. (2007) available at [vizier¹](http://vizier.u-strasbg.fr) in the absolute magnitude range $-25 \lesssim M_V \lesssim -23$. This yielded 42 sources, of which 23 were radio quiet. In order to produce a control sample with a RL fraction closer to that found in optically-selected samples we defined a pure RQ sample of 23 sources supplemented with 3 randomly-selected RL sources that yielded 26 sources in the control sample (the 26 low- z sample will be hereafter referred to as the FOS-CS).

3. Results

Fig. 4 and Fig. 5 show the results of SPECFIT (Kriss 1994) analysis of the $\text{Ly}\alpha$, $\text{Civ}\lambda 1549$ and 1900 blends in individual Pop. A and B sources of the GTC sample. Table 3 reports quantities measured in the rest frame spectra of each source as fol-

lows: rest-frame continuum flux level at 1450\AA and associated uncertainty; total fluxes for the most prominent broad emission features ($\text{Ly}\alpha$, $\text{Nv}\lambda 1240$, $\text{OIV}\lambda 1402 + \text{SiIV}\lambda 1397$, $\text{Civ}\lambda 1549$, $\text{AlIII}\lambda 1860$, $\text{SiIII}\lambda 1892$, $\text{CIII}\lambda 1909$); equivalent widths for $\text{Ly}\alpha$ and $\text{Civ}\lambda 1549$ (equivalent widths for other lines can be estimated by scaling EW $\text{Civ}\lambda 1549$ by line $\text{Civ}\lambda 1549$ flux ratio). Data are presented in two groups: upper Pop. A and lower Pop. B.

Our SPECFIT analysis followed past work modelling $\text{H}\beta$ and $\text{Civ}\lambda 1549$ where strongest results were obtained from studies of $\text{H}\beta$ (at $z < 0.7$) for which the largest body of data exists (Marziani et al. 2003, 2009; Zamfir et al. 2010). As noted in §2.3, past work identified three broad emission components (BLUE, BC and VBC) which show different relative intensities in different sources and are not necessarily present in every individual line/source (Marziani et al. 2010). The “classical” relatively unshifted broad $\text{H}\beta$ component is present in almost all sources and is assumed to be the most reliable virial estimator after $\text{MgII}\lambda 2800$ (Marziani et al. 2013). This is where the Population A-B distinction becomes important. Population A sources involving the highest L/L_{Edd} emitters show a Lorentzian BC component with $\text{FWHM} \leq 4000 \text{ km s}^{-1}$ plus, in extreme sources, a component on the blue side of the BC. Pop. B sources, including most radio-loud quasars, show a BC and a broader redshifted VBC component. In a few cases we suspect that the $\text{H}\beta$ profile may be dominated by the VBC (e.g. PG 1416–129; Sulentic et al. (2000c). Detailed studies of the $\text{Civ}\lambda 1549$ profile in low z quasars are more limited and rely on the ≈ 140 sources with HST archival spectra (Bachev et al. 2004; Sulentic et al. 2007). Pop. A sources show a stronger $\text{Civ}\lambda 1549$ blue component which can be much stronger than the BC (no VBC emission is seen). The well studied NLSy1 source IZw1 is a Pop. A (bin A3) prototype. In some sources a red asymmetry is seen in the CIV profile and is attributed to VBC emission—almost always involving Pop. B sources.

The estimated contribution of the blue component to the total flux of $\text{Civ}\lambda 1549$ is listed in Table 3 under the column labelled F_{blue}/F . Table 4 reports quantities measured from the full broad line profiles (i.e. without separating line components). Following columns of Table 4 list: FWHM $\text{Civ}\lambda 1549$, and other profile shape parameters that provide a quantitative description of $\text{Civ}\lambda 1549$ (see Zamfir et al. 2010 for definitions): asymmetry index, kurtosis, and centroid displacement (with respect to rest frame) at 1/4 and 1/2 fractional intensity.

While we have applied our standard multicomponent SPECFIT analysis to all GTC spectra, the S/N of the data make clear that we could be over-interpreting some of the spectra. We show all individual fits and table derived quantities even though some are uncertain and not directly relevant to the goals of the paper which involve high-low redshift comparisons for Pop A and Pop. B quasars. Subtraction of a blue component from $\text{Civ}\lambda 1549$ is well supported for Pop A sources which also show a mean profile blueshift of $\sim 450 \text{ km s}^{-1}$. However Pop. B sources show no systematic blueshift raising doubts about the reality of a blue component in those sources. Modeling of broader Pop. B line profiles is always more problematic. In the case of Pop. A sources the presence of blue and BC components is well established and no evidence of a VBC is found.

3.1. $\text{Civ}\lambda 1549$ in Population A and B at high and low redshift

$\text{Civ}\lambda 1549$ is the safest feature with which to effect a comparison between low and high redshift. $\text{Civ}\lambda 1549$ is a strong collisional resonance doublet and is not heavily blended with other strong lines. The $\text{Civ}\lambda 1549$ profile shift was chosen as a principal 4DE1

¹ [J/ApJ/666/757/CIVlines](http://vizier.u-strasbg.fr) at <http://vizier.u-strasbg.fr/>

parameter because it showed a strong population A-B difference. EW Civ λ 1549 and Civ λ 1549 profile asymmetry could also serve as 4DE1 diagnostics (Sulentic et al. 2007). Table 6 reports the virial broadening estimator FWHM (see §3.4) and measures of the Civ λ 1549 line profile (FWHM, asymmetry index, kurtosis and centroids at one quarter and half maximum; see Zamfir et al. 2010 for definitions of parameters given here) for the GTC and FOS-CS.

Civ λ 1549 shows striking similarity at high and low redshift in both Pop A and B. The composite spectra show median equivalent width (EW), asymmetry index (AI) and profile shift at half maximum ($c(\frac{1}{2})$) at low and high z that are almost identical (Table 6). We were able to distinguish Pop. A and B on the basis of the same criteria employed at low- z applied to the UV (§2.3 and Negrete et al. 2014), and quantitative Pop. A-B differences in EW and profile measures previously found at low redshift are confirmed in the high redshift GTC sample. Civ λ 1549 in Pop. A sources shows a systematically lower EW than Pop. B as well as blue asymmetric and blueshifted profiles. Pop. B sources show a stronger high ionization spectrum without evidence for profile blueshifts/asymmetries. Pop. B shows an additional very broad and redshifted component with FWHM and shift values similar to those found for H β at low redshift.

Figure 6 compares the Civ λ 1549 equivalent width, centroid shift and FWHM distributions for the high and low redshift samples. Population A and B are identified (Pop. B shaded). Low redshift samples (Bachev et al. 2004; Sulentic et al. 2006) show lower Pop A equivalent widths and FWHM values than Pop. B ($W(\text{Civ}\lambda 1549)_A \approx 50 \text{ \AA}$ vs. $W(\text{Civ}\lambda 1549)_B \approx 83 \text{ \AA}$ and $\text{FWHM}(\text{Civ}\lambda 1549)_A \approx 4060 \text{ km s}^{-1}$ vs. $\text{FWHM}(\text{Civ}\lambda 1549)_B \approx 5810 \text{ km s}^{-1}$). Our high redshift sample shows $W(\text{Civ}\lambda 1549)_A \approx 45 \text{ \AA}$ vs $W(\text{Civ}\lambda 1549)_B \approx 69 \text{ \AA}$ similar to the differences found at low redshift where Pop. A sources generally show a weaker high ionization line spectrum (Marziani et al. 2001, 2010). Note that there is again no significant difference between the $W(\text{Civ}\lambda 1549)$ values between the GTC and FOS-CS. The distribution of Figure 6 show a few (1 – 3, depending on the random selection of radio sources) large equivalent width sources in the FOS-CS that have no correspondence in the GTC sample. They are not numerous enough to make the samples significantly different. Median $\text{FWHM}(\text{Civ}\lambda 1549)$ measures for the high redshift sample are 5010 km s^{-1} and 5830 km s^{-1} for Pop. A and B, respectively roughly consistent with the low- z FOS-CS. However, there is a small discrepancy involving the $\text{FWHM}(\text{Civ}\lambda 1549)$ comparison where high z Pop. A and B average composite widths are about 27% and 10% broader than control sample (CS), respectively. These differences are not statistically significant – given the small sample size and the errors involved. The difference disappears for Pop. B if medians are considered and is reduced to $\approx 15\%$ for Pop. A. Analogous considerations apply to the virial FWHM.

Considering the individual and composite fits to the Civ λ 1549 profile, we do not confirm a near ubiquity of blueshifts/asymmetries for type-1 quasars (Richards et al. 2011) but rather the same Pop. A/B dichotomy seen at low redshift (Sulentic et al. 2007) where Pop. B sources show red shifts/asymmetries or symmetric unshifted profiles.

3.2. Comparing Pop. A and B UV spectra at high and low redshifts

Comparison of Pop. A and B sources at high and low redshift cannot extend beyond the Civ λ 1549 line without use of compos-

ite spectra to enhance spectral S/N. The GTC sample is not large enough ($N = 20$) to permit a fine subdivision so we simply constructed the Pop. A and B median composites that are shown in the upper panel of Fig. 7 that involves 11 and 9 Pop. A and B sources respectively.

The best low z composites come from Bachev et al. (2004). This sample was large enough to permit construction of composite spectra for each of the five most populated 4DE1 bins (Sulentic et al. 2002). The bin composites could then be combined to produce two higher S/N composites for Pop. A and B. Low z Pop. A and B composites shown in the bottom panel of Fig. 7 were obtained by weighting sources from the 5 spectral subtypes by their relative frequency in the sample. These weighted-average composites include all Bachev et al. (2004) spectra. They are the best control sample composites but include many sources that fall outside the narrow luminosity range (almost all lower) of our GTC sample. In order to check on these composites we also generated (lower S/N) composites from our luminosity restricted FOS-CS control sample taken from Sulentic et al. (2007). The Bachev et al. (2004) and Sulentic et al. (2007) samples are largely overlapping with Bachev et al. (2004) including 139 sources vs. 130 of Sulentic et al. (2007). The 26 sources of CS are included in both samples. The luminosity restricted FOS-CS composites show no major differences from the ones obtained from the less restricted Bachev et al. (2004) composites. Neither FOS-CS composite (except for slightly weaker NIII λ 1750 emission in Pop. A). We therefore cautiously adopt the higher S/N Bachev et al. (2004) composites for all comparisons. The two bottom rows of Fig. 8 (the panels labelled B04) present results from SPECFIT analysis of the low- z Bachev et al. (2004) composites for Ly α , Civ λ 1549, and the 1900 blend, and the last two rows of Table 5 report measures derived from this analysis (last two rows identified with the label B04).

If one assumes that source luminosity is the principal driver of quasar structure and kinematics then we expect our low z and GTC composites to be very similar. In fact our work in the 4DE1 context suggests that L/L_{Edd} is the principal driver (Marziani et al. 2001). A comparison of this kind requires the Pop. A and B distinction because quasar spectra are *not* the same and spectral differences at any fixed redshift are maximized using the Pop. A and B distinction which is driven by L/L_{Edd} . We are aware of no more effective distinction. Previous work on low redshift samples show that the two populations divide approximately 60% /40%, with RQ / RL quasars dividing 90 % /10 %, and the wide majority of RLs belonging to Pop. B (Zamfir et al. 2008). If our samples are small or modest as in the present case, an overrepresentation of extreme sources would bias the comparison. There is no reason to expect (and no evidence for) such an overrepresentation. If, for example, many of our sources were soft X-ray selected then we would expect them to preferentially occupy 4DE1 spectral bins A2, A3, A4 which also show the largest and most frequent Civ λ 1549 blueshifts (smallest M_{BH} and highest L/L_{Edd}). Radio selected quasars would largely occupy Pop. B spectral bins. Table 1 suggests that few of our quasars were selected in either way. If anything deep optical grism searches will favor quasars with stronger (broader, higher EW) spectral lines. This might disfavor extreme Pop. A quasars and indeed we find only 2 candidate extreme Pop. A (i.e., narrow line Seyfert 1) sources in the GTC sample (Q1232-1113 and CX-OMPJ20563+0431). Hypothesized to be as younger quasars, we might expect to find more of them at $z \approx 2.3$. High z analogues of I Zw 1 (albeit much higher luminosity) were identified in one of

our companion surveys (Dultzin et al. 2011; Negrete et al. 2012; Marziani & Sulentic 2013; Marziani & Sulentic 2014).

Table 5 reports normalized fluxes and equivalent widths for Pop. A and B composite (average and median) spectra. The spectra are shown in Fig. 7. Note that the measures come from the composite spectra using the same `SPECTFIT` analysis (Fig. 8, top rows) applied to individual sources. Given the sizes of both samples some differences due to outlying/peculiar sources could affect average values/composites; however the mean and median composites yield values that are mutually consistent. Values for Pop. A and B composite spectra are consistent with values derived for the 11 and 9 individual spectra.

In conclusion, following the 4DE1 formalism we attempt a first-order separation of our high- z and low- z samples into Population A and B quasars. In the UV rest wavelength range studied here we find evidence for spectral differences between Pop A and B especially in measures of CIV which is strong and not blended with other strong lines. Table 5 compares high and low redshift median composite spectra for Pop. A and B. Both low- and high- z Pop. B samples show stronger high ionization spectra and stronger narrow lines than Pop. A, while no major difference is found between GTC and the B04 composites.

3.3. Metallicity difference between high and low z ?

One advantage of comparisons involving UV spectra is that they provide several line ratios that can serve as metallicity indicators. Most results of the past decade point toward solar and supersolar metallicity even at very high redshifts (e.g. Hamann & Ferland 1993; Kurk et al. 2007; Willott et al. 2010). Of course these studies involved extremely luminous sources. The GTC sample spectra have high enough S/N to permit reasonable measures of metallicity indicators ($Nv\lambda 1240/Civ\lambda 1549$, $Siv\lambda 1397+Oiv\lambda 1402/Civ\lambda 1549$). The ratio involving nitrogen and carbon scale with metallicity by virtue of the secondary enrichment of nitrogen in massive stars (Hamann & Ferland 1993; Hamann et al. 2002). The ratio $Siv\lambda 1397+Oiv\lambda 1402/Civ\lambda 1549$ involves ionic species of two alpha α elements relative to carbon. The dependence of $Siv\lambda 1397+Oiv\lambda 1402/Civ\lambda 1549$ on Z has been calibrated by photoionization computations (Nagao et al. 2006b) and widely used in recent quasar studies involving metal abundances (e.g., Wang et al. 2012; Shin et al. 2013). The values of the ratios obtained from the fluxes in Table 3 indicate a large spread (at least 0.6dex) in both the $Nv\lambda 1240/Civ\lambda 1549$ and $(Siv\lambda 1397+Oiv\lambda 1402)/Civ\lambda 1549$ ratios (middle and bottom panel of Fig.9). The largest sample presently available for comparison is provided by Shin et al. (2013) who measured $Nv\lambda 1240/Civ\lambda 1549$ and $Siv\lambda 1397+Oiv\lambda 1402/Civ\lambda 1549$ from IUE and HST spectra of PG quasars available in the MAST archive. Fig. 9 compares the GTC distribution of $Nv\lambda 1240/Civ\lambda 1549$ (middle panel) and $(Siv\lambda 1397+Oiv\lambda 1402)/Civ\lambda 1549$ (lower panel) with Shin et al. (2013). Fig. 10 compares GTC measures for $Nv\lambda 1240/Civ\lambda 1549$ (upper panel) and $(Siv\lambda 1397+Oiv\lambda 1402)/Civ\lambda 1549$ with those of Shin et al. (2013) as a function of source bolometric luminosity. The GTC sample overlaps the high- L part of the Shin et al. (2013) sample, where metal richer sources are found (Juarez et al. 2009). The correlation between Z -sensitive ratio $Nv\lambda 1240/Civ\lambda 1549$ and L in Fig. 10 was seen previously (Nagao et al. 2006b) although its origin is unclear (§4.4). In order to make a meaningful comparison between the GTC and low- z samples we applied a restriction to luminosities larger than 10^{45} erg s^{-1} . In this case, there is a consistent difference in the distri-

bution of the ratios, supported by K-S tests, in the sense that the GTC sample sources show lower values.

Metallicity is estimated to be solar or slightly sub-solar in the lowest Z cases. We tentatively identify at least four quasars (F864-158, Q 1340+27, Q 1640+40 and CADIS 16h-1610) that appear to show sub-solar or solar metallicities following the normalization of Nagao et al. (2006b). A low Z for these sources is also suggested by their large $Civ\lambda 1549/CIII\lambda 1909$ ratios (upper panel of Fig.9). This ratio is usually not considered as a metallicity indicator because it is sensitive to ionization level, density (the $CIII\lambda 1909$ line is emitted in an inter-combination transition with a well defined critical density), and because it is the ratio between lines of two different ionic species of the same element. However, for a fixed density (below the critical density of $CIII\lambda 1909$) and ionization parameter, `CLOUDY` (Ferland et al. 2013) photoionization simulations show a remarkable dependence on metallicity for the ratios $CIII\lambda 1909/Civ\lambda 1549$ and $(AlIII\lambda 1860+SiIII\lambda 1892+CIII\lambda 1909)/CIII\lambda 1909$ (Fig. 11). These trends are explained by an increase of electron temperature with decreasing metallicity: at $Z \sim 0.01Z_{\odot}$, $T_e \approx 27000K$, at $Z \sim 5Z_{\odot}$, $T_e \approx 16000$ (assuming $\log U = -1.75 \log n_H = 10$). The higher T_e , due to lower cooling rate of the BLR at low Z , increases the collisional excitation rate of $Civ\lambda 1549$, and therefore favors this line over lower excitation metal lines. It is interesting to note that this interpretation is analogous to ascribing the change in $[OIII]\lambda\lambda 4959,5007$ strength in Galactic and extragalactic HII regions to differences in metal content (e.g., Searle 1971).

An additional line of evidence supports the idea of lower chemical abundance in GTC sources in Pop. A. Fig. 12 shows a comparison of the difference in line width of the Pop. A composite spectra for GTC and FOS sources on an expanded scale to emphasize weak lines. The low- z FOS composite is much richer in faint narrow and semi-broad features. Two emission lines coming from two different ionic species of nitrogen are detected in quasar spectra: $NIII\lambda 1750$ and $NIV\lambda 1486$. We estimate an upper limit of $\approx 0.5\text{\AA}$ for $NIV\lambda 1486$ (the line is not visible) and $W(NIII\lambda 1750)\approx 0.6\text{\AA}$ for the GTC median composite. Both lines are clearly seen in the low- z composites with $W(NIV\lambda 1486)\approx 0.8\text{\AA}$ and $W(NIII\lambda 1750)\approx 1.6\text{\AA}$. The weakness or even absence of both of them in the GTC composites implies lower nitrogen abundance in the high z sources. The $Si III\lambda 1264$, $O II\lambda 1304$ and $O III\lambda 1663$ lines (from α elements), as well as the $Fe II$ UV 191 blend are certainly detected in the FOS composite. The weaker UV 191 $Fe II$ multiplet in the GTC spectrum points toward a clear role for excitation conditions and chemical abundance. Both standard diagnostic line ratios and the comparison of composites are evidence for a metallicity redshift gradient.

3.4. M_{BH} and L/L_{Edd} at high and low z .

Our first attempt to estimate black hole masses and Eddington ratios revealed no significant difference between population A and B sources. We considered virial FWHM values for five UV lines ($Ly\alpha$, $Civ\lambda 1549$, $AlIII\lambda 1860$, $SiIII\lambda 1892$, and $CIII\lambda 1909$) as well as an average FWHM of all five lines. In a few cases not all the lines could be measured. The first line is dangerous for many reasons. The second is our strongest and least contaminated line but different studies suggest it is not reliable as a virial estimator (Sulentic et al. 2007; Netzer et al. 2007). $CIII\lambda 1909$ is seriously blended and similarly FWHM $CIII\lambda 1909$ shows no correlation with FWHM $H\beta$. Recent studies using high S/N spectra (Negrete et al. 2013a; Negrete et al. 2014) suggest

that $\text{AlIII}\lambda 1860$ and $\text{SiIII}\lambda 1892$ are likely the safest virial estimators in UV spectra of quasars. $\text{AlIII}\lambda 1860$ is preferred because it is on the blue edge of the $\lambda 1900$ emission line blend.

We do not report M_{BH} and L/L_{Edd} estimates for individual sources but follow the procedure developed in Sulentic et al. (2002) and Marziani et al. (2009) which involves producing high S/N composite spectra in the 4DE1 context. This was already done for our low- z control sample (Bachev et al. 2004) where composites for the five most populated bins were generated. The size of the GTC sample allows only a simple binning into Pop. A and B sources. Composite spectra are shown in Fig. 7 with SPEC-FIT results in Fig. 8. The GTC binning was partially validated in an earlier section where $\text{CIV}\lambda 1549$ measures for Pop. A and B sources at high- and low- z were compared and found to be very similar. Pop. A – B differences previously established for the low- z sample were also confirmed in the GTC sample. Our best chance for making a reliable comparison of M_{BH} and L/L_{Edd} lies with comparison of the high and low- z composites where the range of source luminosities of both samples is small and similar. Use of composites yields spectra with S/N high enough to resolve the 1900 blend and measure FWHM $\text{AlIII}\lambda 1860$ and $\text{SiIII}\lambda 1892$ with reasonable accuracy. We avoid using the other lines as virial estimators.

Armed with a virial broadening estimator we computed M_{BH} from the standard relation of Vestergaard & Peterson (2006, see Marziani & Sulentic 2012 for a recent review on M_{BH} derivation in quasars). This scaling law is preferred over a more recent formulation (Shen & Liu 2012) because the latter applies most directly to sources with higher luminosity than the ones in our samples. Table 7 presents estimates of M_{BH} and L/L_{Edd} derived using virial FWHM measures listed in Table 6. Values are given for the four median composite spectra displayed in Fig. 7. Median source luminosities are also presented in Table 7. Table 6 also lists FWHM $\text{CIV}\lambda 1549$ values for comparison; making it clear that use of $\text{CIV}\lambda 1549$ as a virial estimator would yield M_{BH} estimates much larger than those derived from FWHM $\text{AlIII}\lambda 1860$ and FWHM $\text{SiIII}\lambda 1892$. It is difficult to fully estimate effects of sample bias in the composite spectra. If the GTC sample is close to random we reasonably expect most sources to occupy 4DE1 bins A1, A2 and B1. The RL fraction ($n=2$ usually pop. B) $\approx 10\%$ is the random expectation. We also identify two candidate extreme pop A sources (possible bin A3). All of these observations coupled with the similarity of Pop. A and B median $\text{CIV}\lambda 1549$ measures, as well as, pop A and B median differences suggest that our samples are reasonably well matched. Bolometric corrections were applied following Elvis et al. (1994) to compute L/L_{Edd} . We confirm the trend found in low z samples where M_{BH} is smaller in Pop. A (than Pop. B) sources by 0.67 dex and 0.27 dex for low z and GTC samples respectively. Median L/L_{Edd} values for Pop. A are 0.33 and 0.46 dex higher than Pop. B at low and high z .

4. Discussion

There are likely significant numbers of quasars at $z = 2.3$ with luminosities ($L_{\text{bol}} \sim 10^{46}$ erg s $^{-1}$) similar to the most luminous local quasars and SDSS-III/BOSS has recently greatly increased their numbers. One assumes that such quasars are increasingly numerous at all redshifts higher than $z \approx 0.6$ (Glikman et al. 2011; Ikeda et al. 2012). The GTC sample shows that their spectra are similar to low z analogues. Our previously defined 4DE1 formalism (Sulentic et al. 2000b, 2007) identified two quasar populations based on optical, UV and X-ray measures. We made a first attempt at identifying Pop. A and B sources in the GTC sample

using previously established criteria including: presence/absence of a $\text{CIV}\lambda 1549$ blueshift/asymmetry, EW CIV (low for Pop. A and high for Pop. B), low/high FWHM $\text{CIV}\lambda 1549$ and line ratios in the 1900 Å blend (Bachev et al. 2004; Sulentic et al. 2007). On this basis, high and low accretors (\propto Eddington ratio) could be tentatively identified. Eddington ratio appears to be the principal driver of 4DE1 differences (e.g., Marziani et al. 2001; Boroson 2002; Yip et al. 2004; Kuraszekiewicz et al. 2009). We find 11 Pop. A and 9 Pop. B sources (omitting the lower z and the red quasar) essentially the same fractional division as observed locally. So far the low L quasar population at $z \approx 2.5$ appears similar to the low z one. The Pop. A – B distinction and spectral differences are preserved. Observational and physical parameters of GTC and the control sample (FOS-CS) are found to be consistent.

4.1. A population of moderately accreting quasars at high redshift: are there real evolutionary effects?

The optical luminosity function for quasars (QLF) based on 2dF or 2QZ is well fit by a pure luminosity evolution model at redshifts lower than the redshift of the peak in the quasar population (e.g., Boyle et al. 2000). At $z \approx 0$ and 2.5 we find turnover absolute magnitude $M_B^* = -22$ and -26 respectively. Thus our samples in the range -23 to -25 are very luminous at low z and underluminous at $z \approx 2.5$. Sources in this luminosity range are still undersampled at $z > 2$ but the first iteration of the BOSS survey (SDSS III: e.g., Palanque-Delabrouille et al. 2013) designed to overcome this deficit requires a double power-law fit to the QLF with pure luminosity evolution up to $z \approx 1 - 2$ and a breakdown at higher z (e.g., Richards et al. 2006). At $z \approx 2 - 2.5$ the onset of the monster quasar population, absent locally, is well developed. The similarity of the $z \approx 2.1 - 2.3$ sample to the local analogues in the control sample supports the interpretation that we are not sampling the monsters but rather the underlying quasar population that grows much more slowly.

Simple expectations for an evolving universe involve an M_{BH} decrease and an L/L_{Edd} increase at higher z (e.g., Kollmeier et al. 2006). A systematic decrease in Eddington ratio after $z \approx 2$ is what is believed to cause the fading of the quasar population (Cavaliere & Vittorini 2000). However, this effect is dominated by the evolution of the most luminous “monster” quasars. If we restrict attention to the less luminous but more numerous population below the OLF turnover luminosity it is at least conceivable that M_{BH} could be systematically smaller (and the Eddington ratio higher) at an age of ≈ 3 Gyr after the Big Bang than in the local Universe.

The luminosity function can be written as

$$\Phi(L, z)dL = \left[\int \Psi(M_{\text{BH}}, z) P\left(\frac{L}{M_{\text{BH}}}|M_{\text{BH}}, z\right) dM_{\text{BH}} \right] dL \quad (1)$$

where $\Psi(M_{\text{BH}}, z)$ is the mass function and P the probability of having a given Eddington ratio at mass M_{BH} at z . GTC and FOS-CS have statistically indistinguishable luminosity distribution; however, this does not rule out the possibility of systematic differences: for example, systematically lower masses and higher L/L_{Edd} at high z .

Our best chance for making a reliable comparison of M_{BH} and L/L_{Edd} lies with comparison of the high and low- z composites where the range of source luminosities is small, and similar, for the two samples. Use of composites make it possible to resolve the 1900 blend and measure FWHM $\text{AlIII}\lambda 1860$ and $\text{SiIII}\lambda 1892$ with higher accuracy. We assigned a luminosity for

the FOS-CS composite from the weighted average of the luminosity of each spectral type used to build the composite itself. We found that M_{BH} derived from median composites at low and high z are consistent.

We also build a distribution using the FWHM $H\beta$ (at low- z , for the FOS-CS) and the “virial FWHM” the GTC sample. Black hole mass values computed following the photoionization method of Negrete et al. (2013a) are consistent with scaling-laws values, with average difference $\delta \log M_{\text{BH}} \approx 0.02 \pm 0.21$. We infer consistent ranges in M_{BH} ($8 \lesssim \log M_{\text{BH}} \lesssim 9$) and L/L_{Edd} at high and low z , if the absolute statistical uncertainty of the single-epoch mass estimates (± 0.66 dex) is taken into account. The L/L_{Edd} systematic difference between Pop. A and B is confirmed at low- and high- z by both the distribution of L/L_{Edd} and by the L/L_{Edd} values estimated from the composite spectra (Table 7). Differences between composite and sample medians are believed to be mainly due to the different assumptions employed to compute M_{BH} and L/L_{Edd} at low and high z .

Our analysis therefore does not provide evidence for a large difference in $\Psi(M_{\text{BH}}, z)$ and $P(\frac{L}{M_{\text{BH}}}, z)$, implying no major effect within the constraints of our small sample. The GTC data allowed us to verify for the first time the presence of a population of moderately accreting quasars with masses and Eddington ratios similar to those seen in the local Universe. This is not ruling out a systematic evolution in the average Eddington ratio with redshift since the massive M_{BH} that were shining at high z have now disappeared and the GTC sample luminosity places them in the high luminosity tail of the local quasar luminosity function (Grazian et al. 2000; Croom et al. 2004). The situation depicted for the quasars at $z \approx 2.3$ indeed appears in close analogy with the ones in the local Universe, where most active black holes have masses in the range $10^8 - 10^9$ solar masses, while less massive black holes $10^6 - 10^7 M_{\odot}$ can be accreting at a higher pace (i.e., they are the local extreme Pop. A sources). In other words, the observation of a similar spread in L/L_{Edd} in the GTC and low- z samples is, within the limit of the present data, consistent with an anti-hierarchical black hole growth scenario (Hasinger et al. 2005; Brandt & Alexander 2010): black holes in the mass range $10^8 - 10^9 M_{\odot}$ are expected to have already acquired a large fraction of their mass at $z \approx 2.4$ and be entering a phase of slower growth (e.g., Marconi et al. 2006). Smaller mass and higher Eddington ratio sources may become more frequent earlier (Kollmeier et al. 2006; Netzer et al. 2007; Trakhtenbrot et al. 2011), or may be simply have been undetected in optical surveys (or even in the soft X-ray domain) at $z \approx 2.4$. This latter case should be seriously taken into account since the one object that is heavily obscured, FIRST/F2M J153150.4+242317, shows properties that are most likely of extreme Pop. A (see discussion in Appendix A). Clearly a larger and less biased sample is needed to gain more constraints on the quasar demographics at $z \approx 2.4$.

4.2. Do Pop. B sources also show $\text{Civ}\lambda 1549$ blueshifts?

We used estimates of $\text{Civ}\lambda 1549$ centroid shift and asymmetry in our separation of high z population A and B sources. Previous work on low redshifts sample found the preponderance of blueshifts in population A sources. The individual shift values listed in Table 4 and composite profile values in Table 6 fully confirm this population A-B difference. We find a few less consistent values in Table 4 which could be explained in several ways: 1) sources misclassified as population A or B, 2) sources with lower S/N spectra where the shift measure is less certain or

3) sources with a somewhat unusual ratio of the BLUE and BC components. The $\text{Civ}\lambda 1549$ line profile in population A sources is composed of at least two components: 1) BLUE- usually attributed to a wind or outflow and 2) BC-a relatively symmetric and unshifted component assumed to be analogous to the primary component seen in $H\beta$ (i.e. the classical BLR used as virial M_{BH} estimator). This is the reason why Pop B sources lacking the BLUE component show FWHM $\text{Civ}\lambda 1549$ values more in agreement with FWHM $H\beta$. Pop A sources without a significant blueshift may involve sources where $\text{Civ}\lambda 1549$ is dominated by emission from the unshifted classical BLR component. The overall consistency of the GTC measures with low z results is impressive.

Analysis of $\text{Civ}\lambda 1549$ profiles in large SDSS samples of quasars (Richards et al. 2011) suggest that $\text{Civ}\lambda 1549$ blueshifts are quasi ubiquitous among the RQ majority of quasars. We do not find this at low redshift where only Pop. A sources show a blueshift. In this paper we also find an absence of pop B blueshifts in the higher redshift GTC sample. The Pop. A-B difference motivated the inclusion of $c(\frac{1}{2})$ as the principal 4DE1 diagnostic involving high ionization broad lines (Sulentnic et al. 2000a). Clearly the Pop. B result for the GTC sample is consistent with zero blueshift. Taken at face value the low redshift results, and now the GTC sample, suggest that about half the quasars show no $\text{Civ}\lambda 1549$ blueshift. Are our results really in conflict with Richards et al. (2011)? Figure 5 of that paper shows the distribution of $\text{Civ}\lambda 1549$ shift vs. $\log L_{\nu}(1550\text{\AA})$ for a large SDSS sample. Of course the S/N of the vast majority of these spectra are inferior to the worst of our data. The centroid of the Richards et al. (2011) distribution lies near $\log L_{\nu} = 30.8 \text{ erg s}^{-1} \text{ Hz}^{-1}$ and $c(\frac{1}{2})(\text{Civ}\lambda 1549) = -800 \text{ km s}^{-1}$ for RQ quasars. $\text{Civ}\lambda 1549$ blueshift decreases rapidly for lower luminosity quasars and our samples concentrate near $\log L_{\nu} \approx 30 \text{ erg s}^{-1} \text{ Hz}^{-1}$ where sources are (as already noted) rare in the SDSS database. The rare equivalent luminosity SDSS quasars in Figure 5 of Richards et al. (2011) show $\text{Civ}\lambda 1549$ shifts between -200 (red) and $+1000$ (blue) km s^{-1} . There is general consistency allowing for the large uncertainties for most of these shift measures and also considering that Richards et al. (2011) do not distinguish between Pop. A and B sources. They do however distinguish between radio-quiet (RQ) and radio-loud (RL) sources. RL sources are largely Pop. B sources in the 4DE1 context and RL sources show a $\text{Civ}\lambda 1549$ centroid blueshift in their Figure 5 (in the L range of our study) of only about 150 km s^{-1} . If RL can be used as a population B surrogate then our results are again roughly consistent with SDSS as explored in Richards et al. (2011). The blueshift results for luminous quasars do not extend to the lower luminosity quasars studied here, which might be an indication that higher luminosity objects are more likely to have a strong wind component.

4.3. Is there a $\text{Civ}\lambda 1549$ evolutionary Baldwin effect?

Since the 1970s there has been interest in the possibility that $\text{Civ}\lambda 1549$ measures might provide a way to use quasars as standard candles for cosmology (c.f. Bian et al. 2012). Interest was sparked by discovery of an apparently strong anticorrelation between EW $\text{Civ}\lambda 1549$ and source luminosity in a sample of RL quasars (Baldwin 1977). EW CIV showed a change from $\log W(\text{Civ}\lambda 1549) \approx 2.1$ at $\log L_{\nu}(1450) \approx 30.0 \text{ erg s}^{-1} \text{ Hz}^{-1}$ to $\log W(\text{Civ}\lambda 1549) \approx 0.9$ at $\log L_{\nu}(1450) \approx 31.9 \text{ erg s}^{-1} \text{ Hz}^{-1}$ (presented with appropriate caution). The history of follow-up studies for this “Baldwin Effect” (Sulentnic et al. 2000a) revealed

an anti-correlation between measures of correlation strength and sample size (decreasing correlation strength with increasing sample size). More recently Eigenvector studies have found that the anticorrelation is most likely intrinsic since quasars at a fixed redshift also show it (Bachev et al. 2004; Baskin & Laor 2004; Marziani et al. 2008). Figure 6 (top panels) show the distributions of $W(\text{CIV}\lambda 1549)$ for our high and low redshift samples. There is no statistically significant difference according to a K-S test. We see the Pop. A-B differences mentioned earlier but no difference in the EW CIV range between the high and low z samples. We find no evidence for a z dependent $W(\text{CIV}\lambda 1549)$ decrease in the GTC sample.

If the GTC measures are compared with the data of Kinney et al. (1990), the GTC values are found to be similar to typical values for low- z quasars with the same luminosity, arguing against an evolutionary Baldwin effect. Overlaying the GTC equivalent width values onto the more recent data of Bian et al. (2012) shows that our sample is consistent with the weak anticorrelation detected in large samples. Small samples like the GTC are however prone to statistical fluctuation. Considering that the Baldwin effect is a rather weak correlation, there is no point in claiming a detection (or a non detection) of a Baldwin effect unless the sample exceeds ~ 100 quasars (Sulentic et al. 2000a). We can just comment that we find the full range of observed $W(\text{CIV}\lambda 1549)$ values even in samples with a restricted luminosity and redshift range: as mentioned, the equivalent width dispersion is here not due to a luminosity correlation since we are studying a sample with essentially fixed luminosity. If $W(\text{CIV}\lambda 1549)$ correlates with luminosity-related parameters it is most likely the source Eddington ratio, i.e., the real effect might be what has been called the “intrinsic” Baldwin effect (e.g., Marziani et al. 2008, 2006).

4.4. Possible interpretation of lower chemical abundance at high z

Several lines of evidence suggest lower chemical abundances in the line emitting gas of the GTC sample with respect to the control sample. This effect – first seen in our sample – was probably never detected before because of the strong correlation between z and L in flux limited samples. It seems unlikely that the strength of inter combination lines with low critical density could be considered a manifestation of the “disappearance” of the NLR observed in some high-luminosity sources (Netzer et al. 2004), since the GTC sample is of ordinary luminosity.

Previous work pointed toward correlation between Z and redshift, luminosity, M_{BH} , and Eddington ratio. A trend involving increasing Z with redshift pointed out in the early mid-1990s has been disproved as associated with Malmquist bias. At present, the better defined correlation of metal content appears to be with luminosity (Shin et al. 2013). This correlation is especially strong, and is confirmed by diagnostics based on narrow lines (Nagao et al. 2006a, 2010). Dietrich et al. (2009) found that gas metallicity of the broad-line region is super-solar with $3 Z/Z_{\odot}$ in luminous, intermediate-redshift quasars, from measures of the $\text{NIII}\lambda 1750/\text{OIII}\lambda 1663$ and $\text{NV}\lambda 1240/\text{CIV}\lambda 1549$ emission line ratios. Also Shin et al. (2013) show a well defined correlation between Z and luminosity for PG quasars at low z . A Z – M_{BH} correlation has been also claimed (Matsuoka et al. 2011), in analogy with what found in galaxies (Matteucci 2012). Last, the possibility of a connection between Z and Eddington ratio has been also explored. Although a connection between Z and L/L_{Edd} is found in the 4DE1 context, as discussed below, the physical origin of this correlation remains unclear, also because the data shown by

Shin et al. (2013) are still insufficient to prove a statistically unbiased correlation.

We must preliminarily point out that great care should be exerted in analyzing data based on the $\text{NV}\lambda 1240/\text{CIV}\lambda 1549$ and $\text{NV}\lambda 1240/\text{HeII}\lambda 1640$ ratios because: (1) the intensity of the $\text{NV}\lambda 1240$ line is very difficult to estimate unambiguously unless a reliable model of the $\text{Ly}\alpha$ wings are built as done by Shin et al. (2013) and in the present paper; (2) the $\text{HeII}\lambda 1640$ profile is often shelf-like, the $\text{HeII}\lambda 1640$ lines is blended with much stronger $\text{CIV}\lambda 1549$ and is therefore difficult to measure accurately especially in low S/N conditions.

The present data suggest a metallicity decrease with z in the same luminosity range.² Within the limits of our sample (a weak anti correlation can be spurious in a small sample: also, the lower Z also rely an even smaller number of sources), lowest metallicity sources have Z values around solar or slightly sub-solar, while other sources show super solar enrichment consistent with the quasar population at the same luminosity. There is a simple interpretation for this finding. The GTC quasars are accreting gas that reflects the chemical composition of the host galaxy; it is known that there is a clear metallicity decrease with z : for fixed host mass $10^{11} M_{\odot}$, the O/H ratio would decrease from 2.5 solar, to 1.5 solar, with a steep decrease with lower host masses (Savaglio et al. 2005). For the typical M_{BH} of our sample, the M_{BH} – bulge mass expected at $z \approx 2.35$ (Merloni et al. 2010; Schulze & Wisotzki 2014) involves stellar masses $\log M_{\star} \sim 11 [M_{\odot}]$. In this case we may well expect metallicity around solar.

The important point here is that we do not have evidence of accretion of “pristine” gas: the metallicity is not highly sub-solar. At the same time, the enrichment is, at least in several cases, not as strong as the one of many luminous quasars: the accreting gas diagnostic ratios are not demanding any enrichment associated with circumnuclear star formation (Sani et al. 2010; Negrete et al. 2012), and may be well ascribed to gas whose metal enrichment has followed the typical processes of the host galaxy of the interstellar medium. In other words, the black hole is being fed by gas whose composition appear normal or close to normal for host galaxies at their cosmic age.

Do these finding allow us to make some more general consideration on the correlations between Z and physical parameters? In the 4DE1 context, there is probably no relation between M_{BH} and Z : the most massive sources in the local Universe, those of Pop. B, do not show evidence of particular enrichment: the metal-content sensitive lines (FeII , $\text{AlIII}\lambda 1860$, $\text{NV}\lambda 1240$) are all the weakest along the 4DE1 sequence. At the other end of the sequence are the highest accretors: they show strong FeII emission and $\text{AlIII}\lambda 1860/\text{SiIII}\lambda 1892 \gtrsim 0.5$ and $\text{SiIII}\lambda 1892 \gtrsim \text{CIII}\lambda 1909$ in the UV (Marziani & Sulentic 2013), and evidence of a large increase in Z , possibly demanding circumnuclear star formation with a top-loaded IMF and/or a special timing in the active nucleus evolution (Negrete et al. 2012). Therefore, a metallicity trend with L/L_{Edd} might be expected. Significant metal enrichment is consistent with a scenario in which the rapidly-accreting phase of the quasar black hole follows gas accumulation, collapse and star formation in the circumnuclear regions (see e.g., Hopkins et al. 2006; Sanders et al. 2009; Teng & Veilleux 2010; Trakhtenbrot et al. 2011). The quasars of the GTC sample do not belong to extreme sources. Their most frequent spectral type is likely A1 or B1, with at most 2 sources whose properties are more consistent with A2/A3. Eddington ratio values are modest,

² Note that this effect is not detectable in the Z -sensitive ratios of Tab. 5 since the median combination of spectra tend to cancel a trend that is seen in a minority of sources.

and mass inflow rates are estimated to be in the range $0.3 - 1 M_{\odot} \text{ yr}^{-1}$. Therefore, the GTC quasars show properties that are consistent with the $Z - L/L_{\text{Edd}}$ relation suggested by the 4DE1 contextualization.

5. Conclusion

We have analyzed GTC spectra for 22 sources near redshift $z \approx 2.35$ using techniques similar to those employed for low- z quasars observed in the UV by HST-FOS. The latter provide an effective comparison sample of luminosity analogues. The properties of the GTC sample are quite similar to the low redshift quasars in the sense that we observe roughly equal numbers of Population A and B high/low accretors. The same Pop. A-B median properties (and Pop. A-B differences) are seen at high and low redshift – this comparison relies on the strong $\text{CIV}\lambda 1549$ line previously selected as a 4DE1 diagnostic. We find no evidence for an “evolutionary” Baldwin effect involving $\text{CIV}\lambda 1549$. We find evidence that the $\text{CIV}\lambda 1549$ blueshift, apparently ubiquitous among high luminosity quasars, is present in only half of both high and low redshift quasars in the moderate luminosity range studied here. It is a high accreting population A property. If Pop. A sources are on average younger by virtue of their smaller inferred M_{BH} (and larger L/L_{Edd} values), our high redshift sample does not show any significant increase in the fraction of “younger” Pop. A sources. However, there is a luminosity selection operating here that lets us miss low M_{BH} sources with M_{BH} significantly below $10^8 M_{\odot}$ even if they are radiating at Eddington limit (with our magnitude limits no source below $\log M_{\text{BH}} \approx 7.5$ should be detectable even with $L/L_{\text{Edd}} \approx 1$).

Evidence for an excess of lower metallicity quasars in the high redshift sample is provided by two diagnostic ratios based on strong emission lines as well as by the overall strength of fainter metal lines in Pop. A sources. These findings are consistent with the evolution of metal content in the stellar populations and presumably in the interstellar medium of the host galaxy.

Acknowledgements. Part of this work was supported by Junta de Andalucía through Grant TIC-114 and Proyecto de Excelencia P08-FQM-4205 as well as by the Spanish Ministry for Science and Innovation through Grant AYA2010-15169. PM wishes to thank the IAA for supporting her visit in March 2014. DD acknowledges support from grant PAPIIT107313, UNAM. Based on observations made with the Gran Telescopio Canarias (GTC), installed in the Spanish Observatorio del Roque de los Muchachos of the Instituto de Astrofísica de Canarias, in the island of La Palma. We thank all the GTC Staff, and especially René Rutten and Antonio Cabrera, for their support with the observations. We would like to thank Josefa Masegosa for all the fruitful discussions on the subject. We also thank the referee for many useful comments which helped to significantly improve the presentation of the GTC survey. This research has made use of the VizieR catalogue access tool, CDS, Strasbourg, France. The original description of the VizieR service was published in A&AS 143, 23. This research has also made use of the NASA/IPAC Extragalactic Database (NED), which is operated by the Jet Propulsion Laboratory, California Institute of Technology, under contract with the National Aeronautics and Space Administration.

References

Ahn, C. P., Alexandroff, R., Allende Prieto, C., et al. 2014, *ApJS*, 211, 17
 Bachev, R., Marziani, P., Sulentic, J. W., et al. 2004, *ApJ*, 617, 171
 Baskin, A. & Laor, A. 2004, *MNRAS*, 350, L31
 Bian, W.-H., Fang, L.-L., Huang, K.-L., & Wang, J.-M. 2012, *MNRAS*, 427, 2881
 Boroson, T. A. 2002, *ApJ*, 565, 78
 Boroson, T. A. 2011, *ApJ*, 735, L14
 Boyle, B. J., Jones, L. R., & Shanks, T. 1991, *MNRAS*, 251, 482
 Boyle, B. J., Shanks, T., Croom, S. M., et al. 2000, *MNRAS*, 317, 1014
 Brandt, W. N. & Alexander, D. M. 2010, *Proceedings of the National Academy of Science*, 107, 7184

Brandt, W. N., Alexander, D. M., Hornschemeier, A. E., et al. 2001, *AJ*, 122, 2810
 Brightman, M., Silverman, J. D., Mainieri, V., et al. 2013, *MNRAS*, 433, 2845
 Brotherton, M. S., Tran, H. D., Becker, R. H., et al. 2001, *ApJ*, 546, 775
 Brühweiler, F. & Verner, E. 2008, *ApJ*, 675, 83
 Cavaliere, A. & Vittorini, V. 2000, *ApJ*, 543, 599
 Cheng, F.-Z., Danese, L., Franceschini, A., & de Zotti, G. 1985, *MNRAS*, 212, 857
 Collin, S., Kawaguchi, T., Peterson, B. M., & Vestergaard, M. 2006, *A&Ap*, 456, 75
 Crampton, D., Janson, T., Durrell, P., Cowley, A. P., & Schmidtke, P. C. 1988, *AJ*, 96, 816
 Crampton, D., Schade, D., & Cowley, A. P. 1985, *AJ*, 90, 987
 Croom, S. M., Smith, R. J., Boyle, B. J., et al. 2001, *MNRAS*, 322, L29
 Croom, S. M., Smith, R. J., Boyle, B. J., et al. 2004, *MNRAS*, 349, 1397
 Dietrich, M., Mathur, S., Grupe, D., & Komossa, S. 2009, *ApJ*, 696, 1998
 Dong, X.-B., Wang, T.-G., Wang, J.-G., et al. 2009, *ApJ*, 703, L1
 Dultzin, D., Martinez, M. L., Marziani, P., Sulentic, J. W., & Negrete, A. 2011, in *Proceedings of the conference “Narrow-Line Seyfert 1 Galaxies and their place in the Universe”*. April 4-6, 2011. Milano, Italy., ed. L. F. et al. (Eds.), *Proceedings of Science*
 Elvis, M., Wilkes, B. J., McDowell, J. C., et al. 1994, *ApJS*, 95, 1
 Eracleous, M. & Halpern, J. P. 2003, *ApJ*, 599, 886
 Fan, X. 2006, *New A Rev.*, 50, 665
 Ferland, G. J., Baldwin, J. A., Korista, K. T., et al. 1996, *ApJ*, 461, 683
 Ferland, G. J., Porter, R. L., van Hoof, P. A. M., et al. 2013, *RevMexA&Ap*, 49, 137
 Glikman, E., Djorgovski, S. G., Stern, D., et al. 2011, *ApJ*, 728, L26
 Glikman, E., Helfand, D. J., White, R. L., et al. 2007, *ApJ*, 667, 673
 Glikman, E., Urrutia, T., Lacy, M., et al. 2012, *ApJ*, 757, 51
 Gordon, K. D. & Clayton, G. C. 1998, *ApJ*, 500, 816
 Gordon, K. D., Clayton, G. C., Misselt, K. A., Landolt, A. U., & Wolff, M. J. 2003, *ApJ*, 594, 279
 Grazian, A., Cristiani, S., D’Odorico, V., Omizzolo, A., & Pizzella, A. 2000, *AJ*, 119, 2540
 Griffith, M. R., Wright, A. E., Burke, B. F., & Ekers, R. D. 1994, *ApJS*, 90, 179
 Hamann, F. & Ferland, G. 1993, *ApJ*, 418, 11
 Hamann, F., Korista, K. T., Ferland, G. J., Warner, C., & Baldwin, J. 2002, *ApJ*, 564, 592
 Hasinger, G., Miyaji, T., & Schmidt, M. 2005, *A&A*, 441, 417
 Hopkins, P. F., Hernquist, L., Cox, T. J., et al. 2006, *ApJS*, 163, 1
 Hu, C., Wang, J.-M., Ho, L. C., et al. 2008, *ApJL*, 683, L115
 Ikeda, H., Nagao, T., Matsuoka, K., et al. 2012, *ApJ*, 756, 160
 Juarez, Y., Maiolino, R., Mujica, R., et al. 2009, *A&Ap*, 494, L25
 Kinney, A. L., Rivolo, A. R., & Koratkar, A. P. 1990, *ApJ*, 357, 338
 Koehler, T., Groote, D., Reimers, D., & Wisotzki, L. 1997, *A&A*, 325, 502
 Kollmeier, J. A., Onken, C. A., Kochanek, C. S., et al. 2006, *ApJ*, 648, 128
 Kriss, G. 1994, *Astronomical Data Analysis Software and Systems III*, A.S.P. Conference Series, 61, 437
 Kuraszkiewicz, J., Wilkes, B. J., Schmidt, G., et al. 2009, *ApJ*, 692, 1180
 Kurk, J. D., Walter, F., Fan, X., et al. 2007, *ApJ*, 669, 32
 Marconi, A., Comastri, A., Gilli, R., et al. 2006, *Mem. Soc. Astron. Italiana*, 77, 742
 Marziani, P., Dultzin, D., & Sulentic, J. W. 2008, in *Revista Mexicana de Astronomia y Astrofisica Conference Series*, Vol. 32, 103
 Marziani, P., Dultzin-Hacyan, D., & Sulentic, J. W. 2006, *Accretion onto Supermassive Black Holes in Quasars: Learning from Optical/UV Observations (New Developments in Black Hole Research)*, 123
 Marziani, P. & Sulentic, J. W. 2012, *New AR*, 56, 49
 Marziani, P. & Sulentic, J. W. 2013, arXiv:1310.3143, *Advances in Space Research* in press
 Marziani, P., & Sulentic, J. W. 2014, arXiv:1405.2727, *MNRAS* in press
 Marziani, P., Sulentic, J. W., Negrete, C. A., et al. 2010, *MNRAS*, 409, 1033
 Marziani, P., Sulentic, J. W., Plauchu-Frayn, I., & del Olmo, A. 2013, *ApJ*, 764
 Marziani, P., Sulentic, J. W., Stirpe, G. M., Zamfir, S., & Calvani, M. 2009, *A&Ap*, 495, 83
 Marziani, P., Sulentic, J. W., Zamanov, R., et al. 2003, *ApJS*, 145, 199
 Marziani, P., Sulentic, J. W., Zwitter, T., Dultzin-Hacyan, D., & Calvani, M. 2001, *ApJ*, 558, 553
 Matsuoka, K., Nagao, T., Marconi, A., Maiolino, R., & Taniguchi, Y. 2011, *A&A*, 527, A100
 Matteucci, F. 2012, *Chemical Evolution of Galaxies (Springer Verlag)*
 Merloni, A., Bongiorno, A., Bolzonella, M., et al. 2010, *ApJ*, 708, 137
 Metzroth, K. G., Onken, C. A., & Peterson, B. M. 2006, *ApJ*, 647, 901
 Nagao, T., Maiolino, R., & Marconi, A. 2006a, *A&A*, 447, 863
 Nagao, T., Maiolino, R., Marconi, A., Matsuoka, K., & Taniguchi, Y. 2010, in *IAU Symposium*, Vol. 267, *IAU Symposium*, ed. B. M. Peterson, R. S. Somerville, & T. Storchi-Bergmann, 73–79
 Nagao, T., Marconi, A., & Maiolino, R. 2006b, *A&Ap*, 447, 157
 Negrete, A., Dultzin, D., Marziani, P., & Sulentic, J. 2012, *ApJ*, 757, 62

- Negrete, C. A., Dultzin, D., Marziani, P., & Sulentic, J. W. 2013a, *ApJ*, 771, 31
Negrete, C. A., Dultzin, D., Marziani, P., & Sulentic, J. W. 2013b *Advances in Space Research* in press (<http://dx.doi.org/j.asr.2013.11.037>)
Negrete, C. A., Dultzin, D., Marziani, P., & Sulentic, J. W. 2014, *ApJ*, accepted
Netzer, H. 2013, *The Physics and Evolution of Active Galactic Nuclei* (Cambridge University Press)
Netzer, H., Lira, P., Trakhtenbrot, B., Shemmer, O., & Cury, I. 2007, *ApJ*, 671, 1256
Netzer, H., Shemmer, O., Maiolino, R., et al. 2004, *ApJ*, 614, 558
Netzer, H. & Trakhtenbrot, B. 2007, *ApJ*, 654, 754
Onken, C. A. & Peterson, B. M. 2002, *ApJ*, 572, 746
Osmer, P. S. & Hewett, P. C. 1991, *ApJS*, 75, 273
Palanque-Delabrouille, N., Magneville, C., Yèche, C., et al. 2013, *A&A*, 551, A29
Papovich, C., Cool, R., Eisenstein, D., et al. 2006, *AJ*, 132, 231
Peterson, B. M. & Wandel, A. 1999, *ApJ*, 521, L95
Richards, G. T., Croom, S. M., Anderson, S. F., et al. 2005, *MNRAS*, 360, 839
Richards, G. T., Kruczek, N. E., Gallagher, S. C., et al. 2011, *AJ*, 141, 167
Richards, G. T., Lacy, M., Storrie-Lombardi, L. J., et al. 2006, *ApJS*, 166, 470
Runnoe, J. C., Brotherton, M., Shang, Z., Wills, B., & DiPompeo, M. 2013, *MNRAS*, 429, 135
Sanders, D. B., Kartaltepe, J. S., Kewley, L. J., et al. 2009, in *Astronomical Society of the Pacific Conference Series*, Vol. 408 *The Starburst-AGN Connection*, ed. W. Wang, Z. Yang, Z. Luo, & Z. Chen, 3
Sani, E., Lutz, D., Risaliti, G., et al. 2010, *MNRAS*, 403, 1246
Savaglio, S., Glazebrook, K., Le Borgne, D., et al. 2005, *ApJ*, 635, 260
Schmidt, M. 1968, *ApJ*, 151, 393
Schmidt, M. & Green, R. F. 1983, *ApJ*, 269, 352
Schmidt, M., Schneider, D. P., & Gunn, J. E. 1995, *AJ*, 110, 68
Schneider, D. P., Richards, G. T., Hall, P. B., et al. 2010, *AJ*, 139, 2360
Schulze, A. & Wisotzki, L. 2014, *MNRAS*, 438, 3422
Searle, L. 1971, *ApJ*, 168, 327
Shemmer, O., Netzer, H., Maiolino, R., et al. 2004, *ApJ*, 614, 547
Shen, Y. & Liu, X. 2012, *ApJ*, 753, 125
Shin, J., Woo, J.-H., Nagao, T., & Kim, S. C. 2013, *ApJ*, 763, 58
Silverman, J. D., Green, P. J., Barkhouse, W. A., et al. 2005, *ApJ*, 618, 123
Sulentic, J., Marziani, P., & Zamfir, S. 2011, *Baltic Astronomy*, 20, 427
Sulentic, J. W., Bachev, R., Marziani, P., Negrete, C. A., & Dultzin, D. 2007, *ApJ*, 666, 757
Sulentic, J. W., Marziani, P., & Dultzin-Hacyan, D. 2000a, *ARA&A*, 38, 521
Sulentic, J. W., Marziani, P., Zamanov, R., et al. 2002, *ApJL*, 566, L71
Sulentic, J. W., Zwitter, T., Marziani, P., & Dultzin-Hacyan, D., 2000b, *ApJL*, 536, L5
Sulentic, J. W., Marziani, P., Zwitter, T., Dultzin-Hacyan, D., & Calvani, M. 2000c, *ApJL*, 15, L15
Sulentic, J. W., Repetto, P., Stirpe, G. M., et al. 2006, *A&Ap*, 456, 929
Sulentic, J. W., Zamfir, S., Marziani, P., et al. 2003, *ApJL*, 597, L17
Sulentic, J. W., Zamfir, S., Marziani, P., & Dultzin, D. 2008, in *Revista Mexicana de Astronomia y Astrofisica Conference Series*, Vol. 32, 51–58
Teng, S. H. & Veilleux, S. 2010, *ApJ*, 725, 1848
Trakhtenbrot, B., Netzer, H., Lira, P., & Shemmer, O. 2011, *ApJ*, 730, 7
Véron-Cetty, M.-P. & Véron, P. 2010, *A&A*, 518, A10
Vestergaard, M. & Peterson, B. M. 2006, *ApJ*, 641, 689
Vestergaard, M. & Wilkes, B. J. 2001, *ApJS*, 134, 1
Wang, H., Zhou, H., Yuan, W., & Wang, T. 2012, *ApJ*, 751, L23
Weedman, D. W. 1985, *ApJS*, 57, 523
Willott, C. J., Delorme, P., Reylé, C., et al. 2010, *AJ*, 139, 906
Wolf, C., Meisenheimer, K., Röser, H.-J., et al. 1999, *A&A*, 343, 399
Yip, C. W., Connolly, A. J., Vanden Berk, D. E., et al. 2004, *AJ*, 128, 2603
York, D. G., Khare, P., Vanden Berk, D., et al. 2006, *MNRAS*, 367, 945
Zamfir, S., Sulentic, J. W., & Marziani, P. 2008, *MNRAS*, 387, 856
Zamfir, S., Sulentic, J. W., Marziani, P., & Dultzin, D. 2010, *MNRAS*, 403, 1759
Zhou, H., Wang, T., Yuan, W., Lu, H., Dong, X., Wang, J., & Lu, Y., 2006, *ApJS*, 166, 128

Table 1. Source Identification and Basic Properties

NED Identification	m_V^a	z	δz	M_B^b	Discovery	Ref.	Alternate Name	Notes
OH91 073	20.9	2.2630	0.0016	-24.4	grism/grens	1	NVSS J121848-110332, Q 1216-1046	NVSS 38.9±1.6 mJy, RL serendipitous
OH91 119	20.9	2.2660	0.0005	-24.4	grism/grens	1	Q 1232-1059	
OH91 121	21.0	2.4065	0.0027	-23.8	grism/grens	1	Q 1232-1113	
B1.0334	21.6	2.2999	0.0012	-23.7	X-ray	2	SDSS J123742.52+621811.6	
Wee 87	20.8	2.2418	0.0022	-24.3	grism/grens	3	HB89 1257+357	
HB89 1340+277	21.4	2.1842	0.0023	-23.7	grism/grens	3	Q 1340+2744	
2QZ J134206.3-003702	20.3	2.2115	0.0028	-24.4	color (2dF)	4	SDSS J134206.34-003701.2	
F864:158	21.7	2.2297	0.0023	-23.4	color	5	SDSS J134423.95-002846.4	
2QZ J143400.0+002649	20.8	2.2054	0.0005	-24.3	color (2dF)	6		
FIRST J153150.4+242317	20.5	2.2841	0.0011	-24.7	IR	7	SDSS/F2M J153150.4+242317	Heavily obscured; RL serendipitous
TXS 1529-230	21.4	2.2800	0.0020	-23.8	Radio	8	PMN J1532-2310	NVSS 138.9±4.2 mJy
CADIS 16h-1610	20.8	2.2717	0.0016	-24.2	color + FP?	9	SDSS J162359.21+554108.7	
CADIS 16h-1373	21.9	2.2780	0.0018	-23.2	color + FP?	9	SDSS J162421.29+554243.0	
Wee 155	21.0	1.5981	0.0049	-24.2	grism/grens	3	HB89 1634+332	$z \approx 2.37$ in catalogues
SDSS J164226.90+405034.3	20.4	2.3258	0.0005	-25.0	grism/grens	10	Q 1640+4056	
SPIT 17196+5922	20.7	2.2255	0.0015	-24.1	IR/Spitzer	11	SDSS J171941.24+592242.1	
VCV96 1721.4+3401	20.9	2.3244	0.0055	-24.1	grism/grens	12	Q 1721+3400	
Wee 173	20.2	2.4144	0.0016	-25.3	grism/grens	3	HB89 1834+509	
Wee 174	20.6	2.2720	0.0008	-24.8	grism/grens	3	HB89 1835+509	
CXOMP J205620.5-043100	21.2	2.3299	0.0032	-23.6	X-ray	13	CXO J205620.5-043100	
VCV96 2240.7+0066	20.4	2.2579	0.0019	-24.5	grism/grens	12	Q 2240+0066	
CXOMP J234752.5+010306	20.5	2.4043	0.0014	-24.3	X-ray	13	SDSS J234752.55+010305.0	

^a Indicative V magnitudes as reported by Véron-Cetty & Véron (2010).

^b Absolute B magnitude at $z = 0$ as tabulated by Véron-Cetty & Véron (2010).

1: Osmer & Hewett (1991); 2: Brandt et al. (2001); 3: Weedman (1985); 4: Croom et al. (2001); 5: Boyle et al. (1991); 6: Croom et al. (2004); 7: Glikman et al. (2007); 8: Griffith et al. (1994); 9: Wolf et al. (1999); 10: Crampton et al. (1988); 11: Papovich et al. (2006); 12: Crampton et al. (1985); 13: Silverman et al. (2005)

Table 2. Log of Observations

QSO Identification	Date Observation	ET Time (s)	Exp. N.	S/N at 1450Å	Slit width (arcsecs)	seeing (arcsecs)
[OH91] 073	26-03-2011	2400	4	14	1.0	1.55
[OH91] 119	26-03-2011	2400	4	10	1.0	1.3
[OH91] 121	07-04-2011	2400	4	20	1.0	1.0
B1.0334	07-04-2011	2400	4	10	1.0	1.15
Wee 87	07-04-2011	2400	4	30	1.0	0.99
[HB89] 1340+277	02-05-2013	2400	4	5	1.0	1.0
2QZ J134206.3-003702	02-05-2011	2400	4	12	1.0	0.98
F864:158	06-05-2011	2400	4	5	1.0	1.3
2QZJ143400.0+002649	05-05-2013	2600	4	11	1.23	1.27
FIRST J153150.46+242317.7	02-05-2011	2400	4	9	1.0	0.80
TEX 1529-230	07-06-2011	2400	4	6	1.0	1.56
CADIS 16h-1610	08-07-2013	3250	5	12	1.23	0.97
CADIS 16h-1373	14-06-2013	3250	5	10	1.23	0.82
Wee 155	02-05-2011	2400	4	5	1.0	1.10
SSDS J164226.90+405034.3	08-04-2011	2400	4	6	1.0	1.25
SPIT 17196+5922	06-04-2011	2400	4	11	1.0	1.01
[VCV96] 1721.4+3401	06-05-2013	2600	4	7	1.23	1.15
Wee 173	05-05-2013	2600	4	40	1.23	0.99
Wee 174	11-06-2013	2600	4	21	0.8	1.2
CXOMP J205620.5-043100	04-07-2011	2400	4	8	1.0	1.15
[VCV96] 2240.7+0066	03-07-2011	2400	4	14	1.0	1.20
CXOMP J234752.5+010306	11-06-2013	2600	4	12	0.8	0.8

Table 3. Measured Quantities

NED Identification	f_λ^a	δf_λ	Ly α		Nv F^c	Oiv]+Siv F^c	Civ λ 1549			AlIII F^c	SiIII] F^c	CIII] F^c	λ 1900 F^c
			W [Å] ^b	F^c			W [Å] ^b	F^c	F_{blue}/F				
Population A													
OH91 119	0.35	0.04	58	23.3	9.6	4.0	36	10.8	0.38	0.7	1.8	3.2	5.7
OH91 121	1.24	0.06	55	80.4	23.9	14.0	37	42.5	0.20	3.5	9.6	5.6	18.8
Wee 87	1.29	0.06	90	153.3	27.0	10.5	51	59.8	0.09	2.7	5.4	13.8	21.9
F864:158	0.16	0.03	137	27.4	5.9	2.0	72	11.2	0.20	0.5	1.1	1.8	3.4
2QZ J143400.0+002649	0.61	0.06	68	52.1	7.9	4.4	26	15.6	0.11	1.1	4.4	4.5	10.0
SPIT 17196+5922	0.76	0.07	66	65.5	16.2	6.0	48	32.3	0.11	2.0	5.1	7.8	14.9
Wee 173	2.36	0.21	89	261.7	34.0	17.0	44	100.5	0.09	1.0	6.4	15.9	23.3
Wee 174	0.44	0.02	70	37.4	7.8	3.6	47	19.7	0.06	0.2	1.3	4.0	5.5
CXOMP J205620.5-043100	0.26	0.04	89	24.8	8.8	4.3	51	12.9	0.31	1.7	4.1	2.8	8.6
VCV96 2240.7+0066	0.66	0.05	101	73.7	11.1	8.0	50	29.6	0.19	1.5	3.2	8.2	13.0
CXOMP J234752.5+010306	0.36	0.03	144	49.9	4.8	2.9	46	17.4	0.10	1.8	2.5	5.1	9.4
Population B													
OH91 073	0.41	0.03	87	44.1	10.2	6.8	75	27.4	0.08	1.0	1.5	4.7	10.6
B1.0334	0.40	0.05	73	41.9	9.6	7.6	118	39.0	0.14	1.1	1.5	5.2	11.8
HB89 1340+277	0.12	0.03	252	20.5	1.4	1.8	141	14.4	0.17	0.5	0.5	1.3	2.7
2QZ J134206.3-003702	0.48	0.04	72	47.7	6.5	6.1	47	19.9	0.20	2.8	3.4	8.5	18.9
TEX 1529-230	0.51	0.08	72	36.7	21.2	6.5	64	31.6	0.02	0.6	2.6	6.8	13.4
CADIS 16h-1610	0.38	0.03	77	42.2	9.3	6.8	59	19.5	0.10	1.4	2.6	5.4	11.8
CADIS 16h-1373	0.11	0.02	277	27.3	5.8	1.5	129	13.2	0.09	0.6	0.8	2.6	5.2
SDSS J164226.90+405034.3	0.31	0.06	132	60.1	4.2	2.9	79	19.4	0.07	0.3	0.7	1.3	2.8
VCV96 1721.4+3401	0.27	0.04	77	27.8	7.4	4.3	90	19.5	0.32	0.8	1.9	2.9	6.5

^a Rest frame specific flux at 1450 Å in units of 10^{-15} erg s⁻¹ cm⁻² Å⁻¹.

^b Rest frame equivalent width in Å.

^c Rest frame flux in units of 10^{-15} erg s⁻¹ cm⁻².

Table 4. Measured C IV λ 1549 Line Profile Quantities

NED Identification	FWHM(C IV λ 1549) [km s $^{-1}$]	A.I.	Kurt.	$c(\frac{1}{4})$ [km s $^{-1}$]	$c(\frac{1}{2})$ [km s $^{-1}$]
Population A					
OH91 119	4510 \pm 260	-0.17 \pm 0.06	0.41 \pm 0.05	-1270 \pm 210	-1170 \pm 130
OH91 121	6990 \pm 370	-0.18 \pm 0.06	0.37 \pm 0.07	-1060 \pm 320	-1160 \pm 190
Wee 87	4610 \pm 390	-0.14 \pm 0.09	0.31 \pm 0.04	-390 \pm 360	-50 \pm 190
F864:158	4880 \pm 540	-0.26 \pm 0.07	0.28 \pm 0.04	-830 \pm 290	-380 \pm 270
2QZ J143400.0+002649	4800 \pm 930	-0.23 \pm 0.07	0.26 \pm 0.03	-1130 \pm 320	-500 \pm 470
SPIT 17196+5922	5160 \pm 400	-0.11 \pm 0.08	0.33 \pm 0.04	-480 \pm 340	-330 \pm 200
Wee 173	4230 \pm 350	-0.21 \pm 0.11	0.27 \pm 0.04	-1130 \pm 470	-310 \pm 170
Wee 174	5070 \pm 360	-0.04 \pm 0.08	0.34 \pm 0.04	-210 \pm 350	-200 \pm 180
CXOMP J205620.5-043100	6240 \pm 280	-0.07 \pm 0.06	0.49 \pm 0.04	-820 \pm 270	-950 \pm 140
VCV96 2240.7+0066	5300 \pm 340	-0.08 \pm 0.07	0.37 \pm 0.05	-490 \pm 310	-490 \pm 170
SDSS J234752.55+010305.0	5600 \pm 620	-0.19 \pm 0.08	0.28 \pm 0.03	-900 \pm 390	-260 \pm 310
Population B					
OH91 073	4170 \pm 250	-0.02 \pm 0.11	0.38 \pm 0.05	130 \pm 360	190 \pm 130
B1.0334	7580 \pm 580	0.08 \pm 0.09	0.31 \pm 0.04	530 \pm 650	-10 \pm 290
HB89 1340+277	4620 \pm 280	-0.13 \pm 0.18	0.35 \pm 0.07	-860 \pm 740	-360 \pm 140
SDSS J134206.34-003701.2	6880 \pm 440	0.00 \pm 0.07	0.38 \pm 0.04	-220 \pm 410	-250 \pm 220
TEX 1529-230	5840 \pm 340	0.11 \pm 0.10	0.39 \pm 0.05	1040 \pm 490	640 \pm 170
CADIS 16h-1610	5930 \pm 340	-0.03 \pm 0.08	0.40 \pm 0.05	10 \pm 370	110 \pm 170
CADIS 16h-1373	5460 \pm 310	-0.01 \pm 0.08	0.41 \pm 0.05	-10 \pm 310	40 \pm 150
SDSS J164226.90+405034.3	3180 \pm 180	0.00 \pm 0.07	0.42 \pm 0.04	-100 \pm 180	-110 \pm 90
VCV96 1721.4+3401	8740 \pm 490	0.12 \pm 0.06	0.43 \pm 0.04	-120 \pm 410	-650 \pm 240

Table 5. Measured Quantities on Composite Spectra

NED Identification	Ly α		Nv	Orv]+Sirv	Civ λ 1549			AlIII	SiIII]	CIII]	λ 1900
	W [Å] ^b	F ^c	F ^c	F ^c	W [Å] ^b	F ^c	F _{blue} /F	F ^c	F ^c	F ^c	F ^c
Pop. A Average	78	87	19.1	8.4	46	42.9	0.10	1.9	7.3	8.5	17.7
Pop. B Average	84	103.0	38.3	13.9	77	69.3	0.09	3.6	7.0	13.3	30.5
Pop. A Median	74	80.0	16.7	9.0	45	42.7	0.18	1.8	5.8	6.6	14.1
Pop. B Median	121	131.5	26	13.0	69	62.2	0.07	3.1	3.9	14.5	26.0
Pop. A B04	87	107.7	15	13.9	51	49.7	0.13	2.5	5.4	11.4	19.3
Pop. B B04	95	115.9	27	11.5	83	77.5	0.11	2.6	3.5	13.0	23.5

^a Rest frame specific flux at 1450 Å in units of ergs s⁻¹ cm⁻²Å⁻¹.

^b Rest frame equivalent width in Å.

^c Rest frame flux in units of ergs s⁻¹ cm⁻².

Table 6. Measured Line Profile Quantities on Composite Spectra

NED Identification	Virial FWHM ^a [km s ⁻¹]	FWHM(Civ λ 1549) ^b [km s ⁻¹]	A.I. ^c	Kurt. ^c	$c(\frac{1}{4})^c$ [km s ⁻¹]	$c(\frac{1}{2})^c$ [km s ⁻¹]
Pop. A Average	3470:	5220 \pm 430	-0.12 \pm 0.08	0.32 \pm 0.04	-730 \pm 370	-440 \pm 220
Pop. B Average	5080	6290 \pm 380	0.01 \pm 0.09	0.39 \pm 0.05	10 \pm 460	-20 \pm 190
Pop. A Median	2880 \pm 320 ^a	5010 \pm 390	-0.10 \pm 0.10	0.31 \pm 0.04	-570 \pm 430	-270 \pm 200
Pop. B Median	4430	5830 \pm 350	0.02 \pm 0.10	0.38 \pm 0.05	350 \pm 450	270 \pm 170
Pop. A B04	2430 \pm 100	4060 \pm 400	-0.15 \pm 0.09	0.31 \pm 0.04	-770 \pm 310	-500 \pm 200
Pop. B B04	4300	5810 \pm 450	0.00 \pm 0.12	0.36 \pm 0.06	10 \pm 590	-10 \pm 230

^a Virial FWHM measured on AlIII λ 1860 and SiIII λ 1892 in accordance with the finding of Negrete et al. (2013a). The uncertainty is the standard deviation computed on the two lines FWHM. If no uncertainty is given, the fit was obtained with the same FWHM value for both AlIII λ 1860 and SiIII λ 1892.

^b FWHM of the Civ λ 1549 line measured on the full profile, i.e., including BC and VBC and BLUE when appropriate.

^c Measures of the Civ λ 1549 full line profile asymmetry index, kurtosis and centroids at one quarter and half maximum on; see Zamfir et al. 2010 for definitions of parameters.

Table 7. M_{BH} and L/L_{Edd} estimates from composite spectra

Spectrum	$\log \lambda L_{\lambda}^{\text{a}}$ [erg s ⁻¹]	$\log L$ [erg s ⁻¹]	$\log M_{\text{BH}}$ [M_{\odot}]	$\log L/L_{\text{Edd}}$
Pop. A median	45.49	45.99	8.37	-0.56
Pop. B median	45.30	45.80	8.64	-1.02
Pop. A B04 composite	45.03	46.03	8.19	-0.35
Pop. B B04 composite	45.46	46.47	8.86	-0.62

^a V luminosity for the B04 composites and 1450 Å λL_{λ} for the GTC medians.

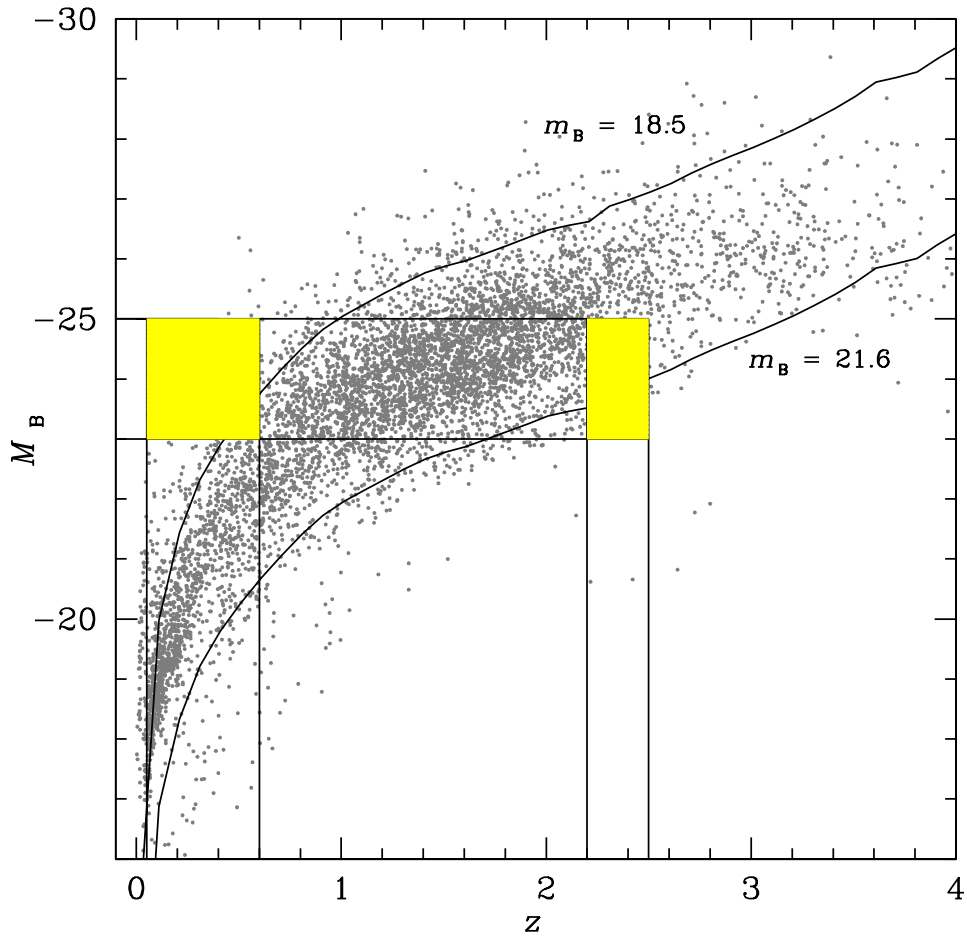


Fig. 1. Absolute magnitude of quasars vs. redshift for the SDSS-based catalog of Schneider et al. (2010). Curves are computed for two limiting (K-corrected) apparent magnitudes $m_B = 18.5$ and $m_B = 21.6$. The shaded boxes identify the loci in the $z - M_B$ planes of two volume limited sample within the same luminosity limits: one between $2.2 \leq z \leq 2.5$ as for the GTC sample of this paper, and a control sample at $0.05 \leq z \leq 0.6$.

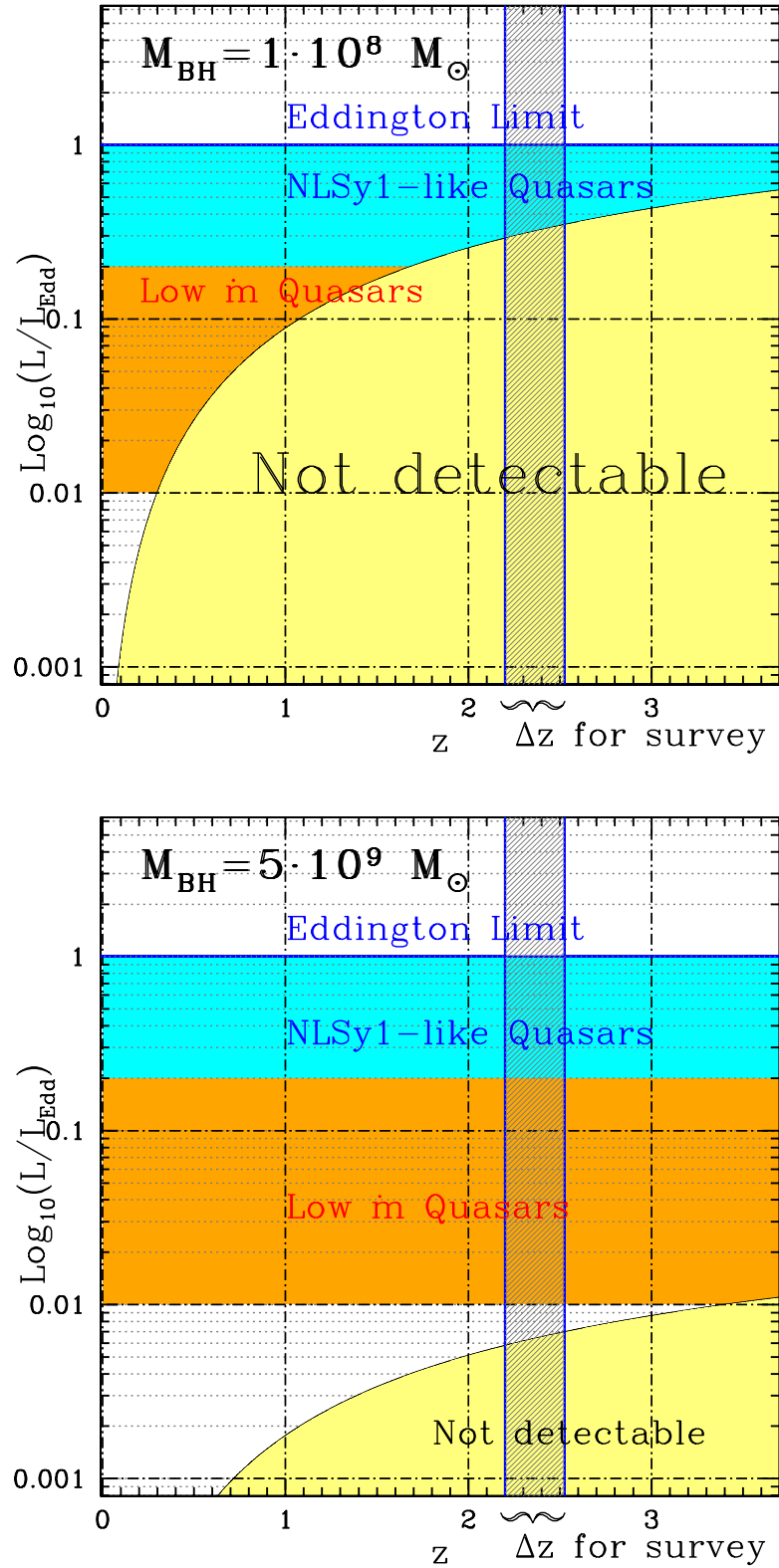


Fig. 2. Eddington ratio as a function of redshift, with the area of undetectable sources below a limiting magnitude $m_B \approx 21.5$) colored in yellow. The redshift range of the quasar survey is identified by the dashed strip. See text for further details.

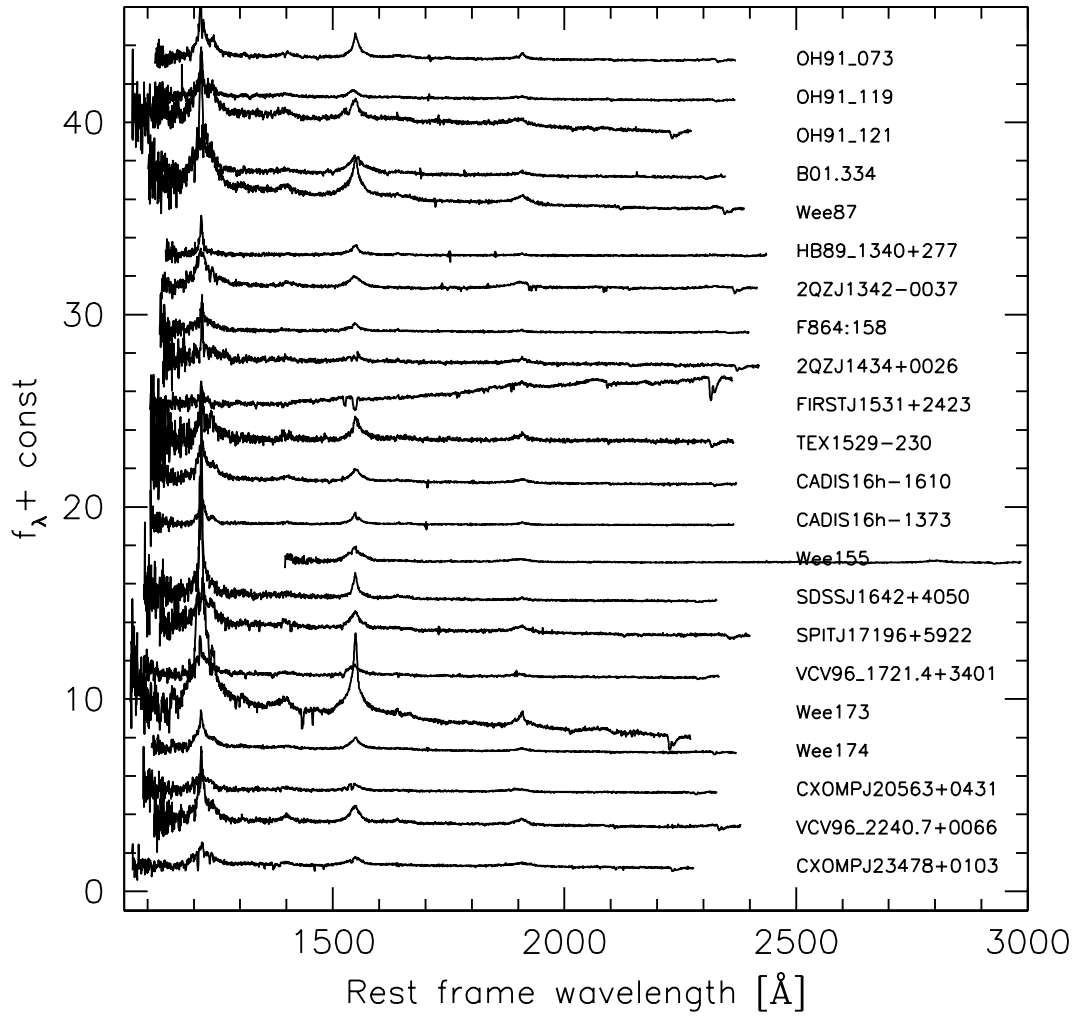


Fig. 3. The GTC quasar spectra after redshift correction. Abscissa is the rest frame wavelength in \AA , ordinate is specific flux in units of $10^{-15} \text{ erg s}^{-1} \text{ cm}^{-2} \text{ \AA}^{-1}$. Spectra have been vertically displaced by adding steps of $\Delta f_\lambda = 2$ (no step was added for Wee 173 to avoid confusion with VCV96 from bottom to top).

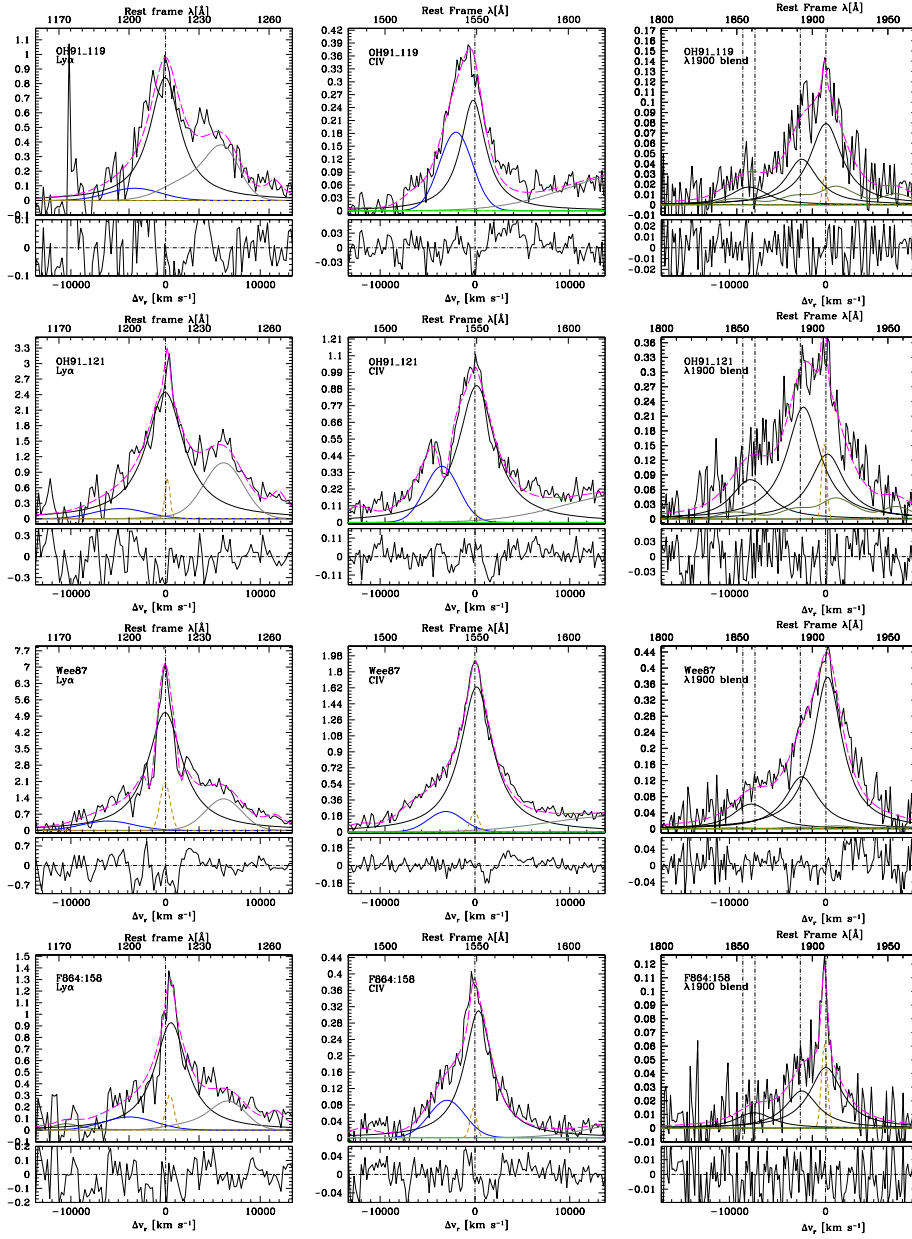


Fig. 4. Results of line fit analysis on the $\text{Ly}\alpha$ (left panel) $\text{CIV}\lambda 1549$ (middle) and 1900 \AA emission features for Pop. A sources. The lines are shown after continuum subtraction. The magenta dashed line show the full model of the emission features and intervening narrow absorptions if present. The thick black lines show the broad components of the prominent emission lines. The thick blue line traces the BLUE component. The $\text{Nv}\lambda 1240$ line on the red side of the $\text{Ly}\alpha$ profile is traced by a grey line that includes its BC and BLUE. Orange lines are narrow line components. The lower panel of each frame shows the residuals between the line model and the observations as a function of radial velocity from rest frame (for $\text{CIII}\lambda 1909$ in the case of the 1900 \AA blend).

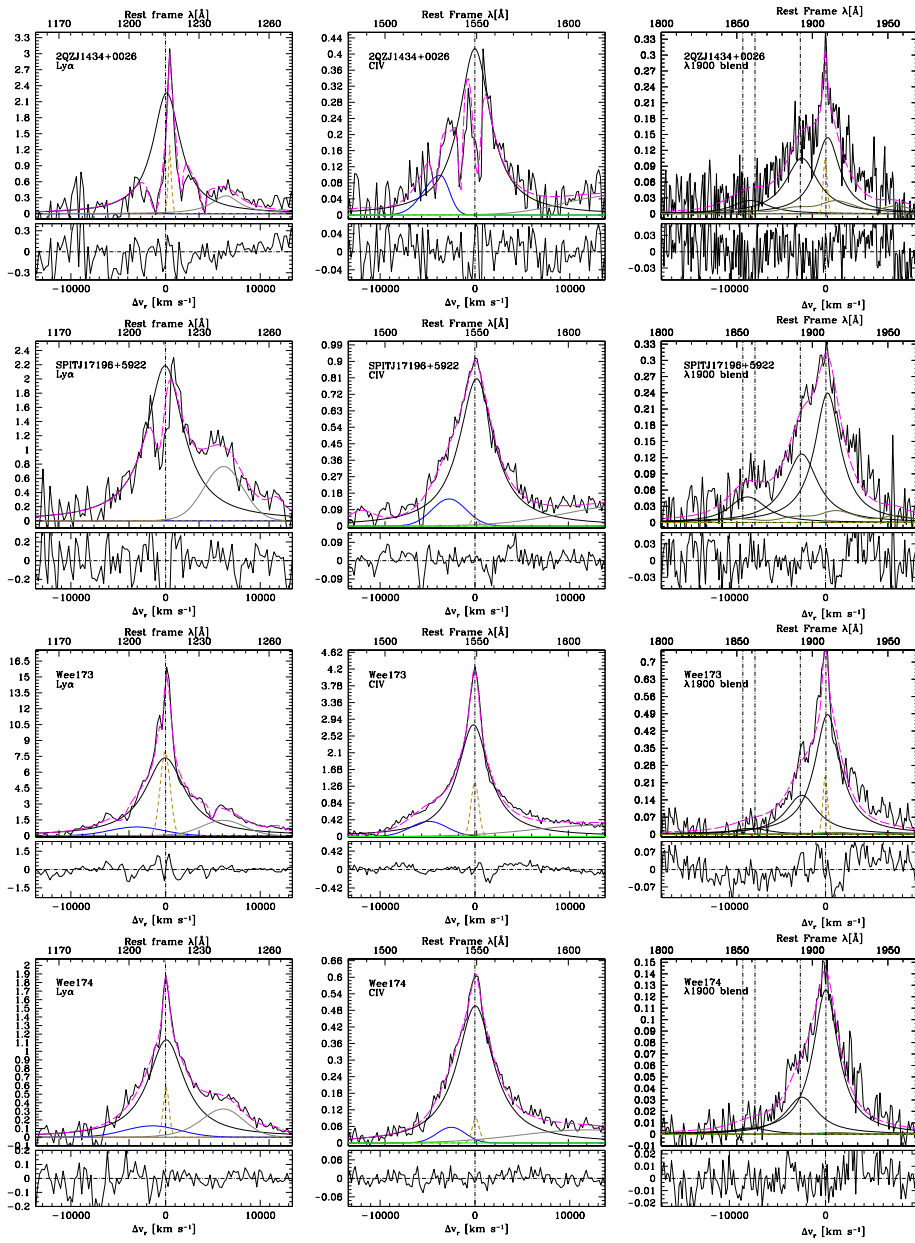


Fig. 4. (cont.)

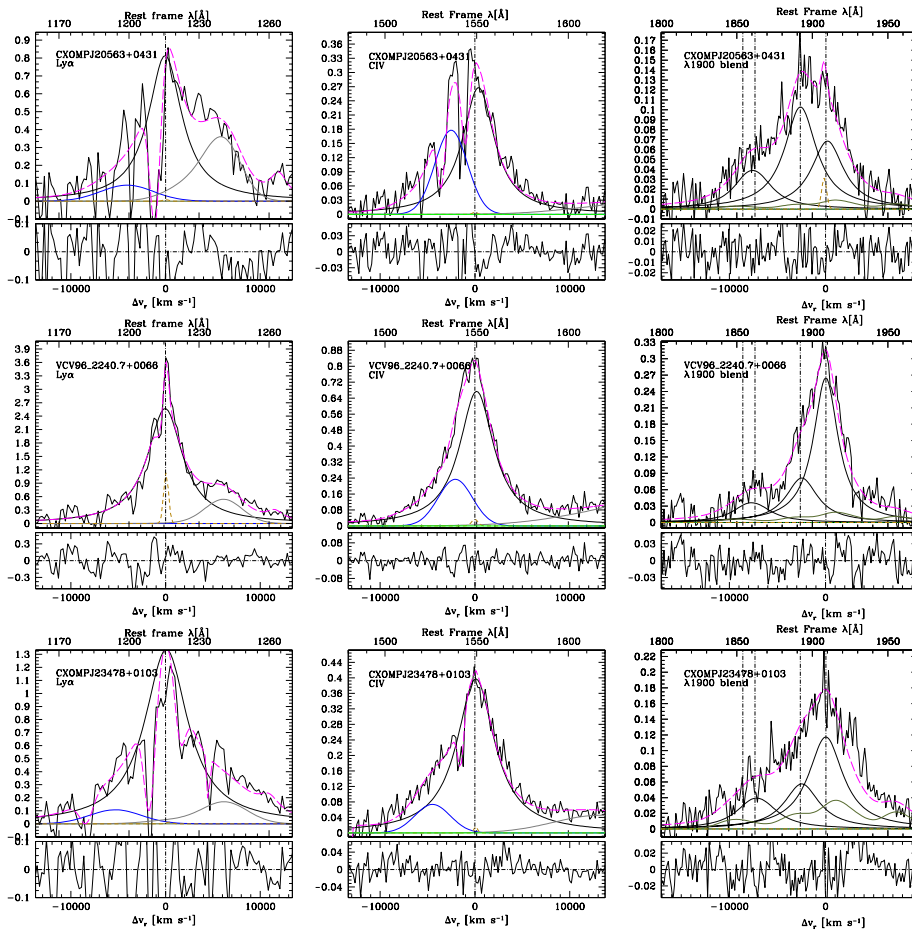


Fig. 4. (cont.)

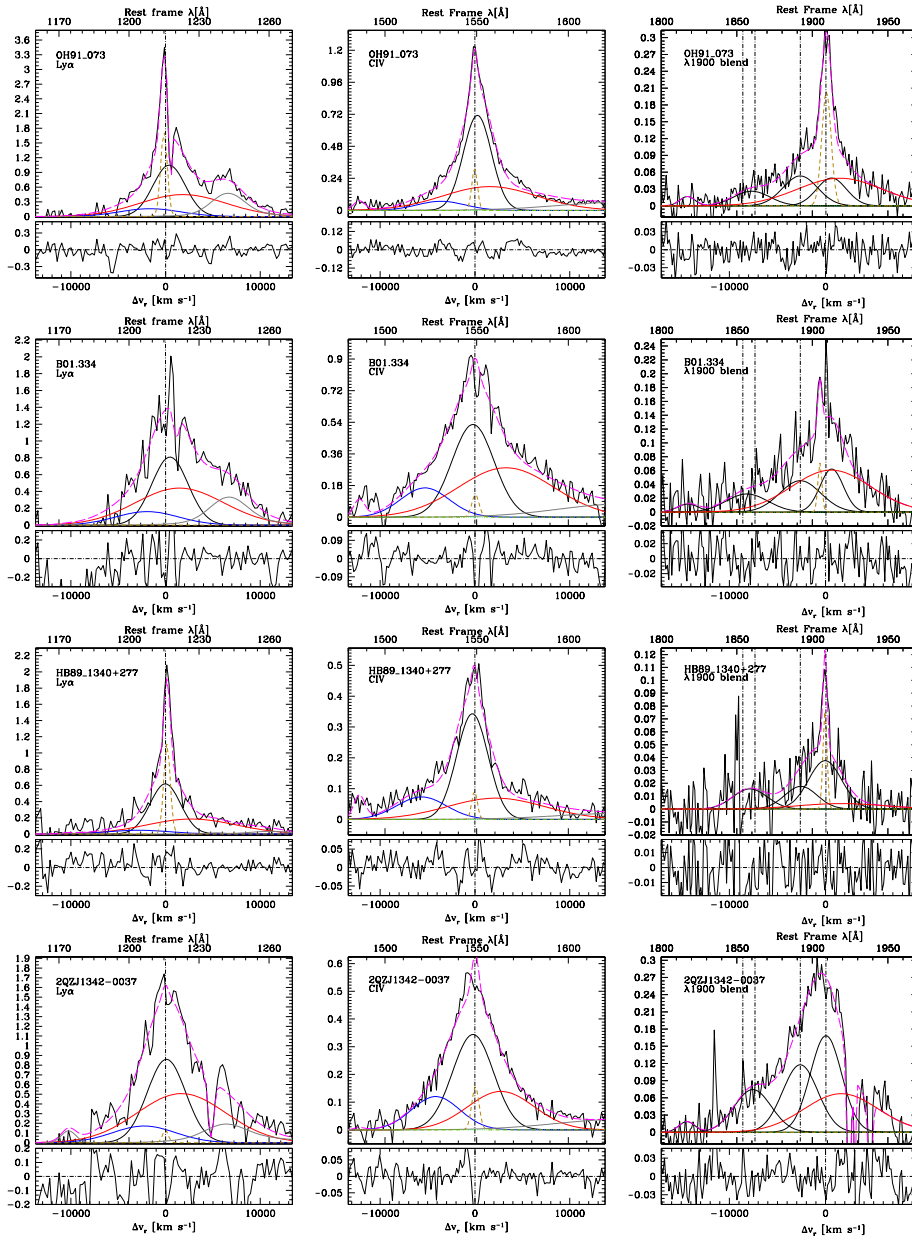


Fig. 5. Results of line fit analysis on the $\text{Ly}\alpha$ (left panel) $\text{CIV}\lambda 1549$ (middle) and 1900 \AA emission features for Pop. B sources. Meaning of symbols and colors is as in the previous Figure. The VBC assumed to be present in the Pop. B emission line profiles is traced by a thick red line.

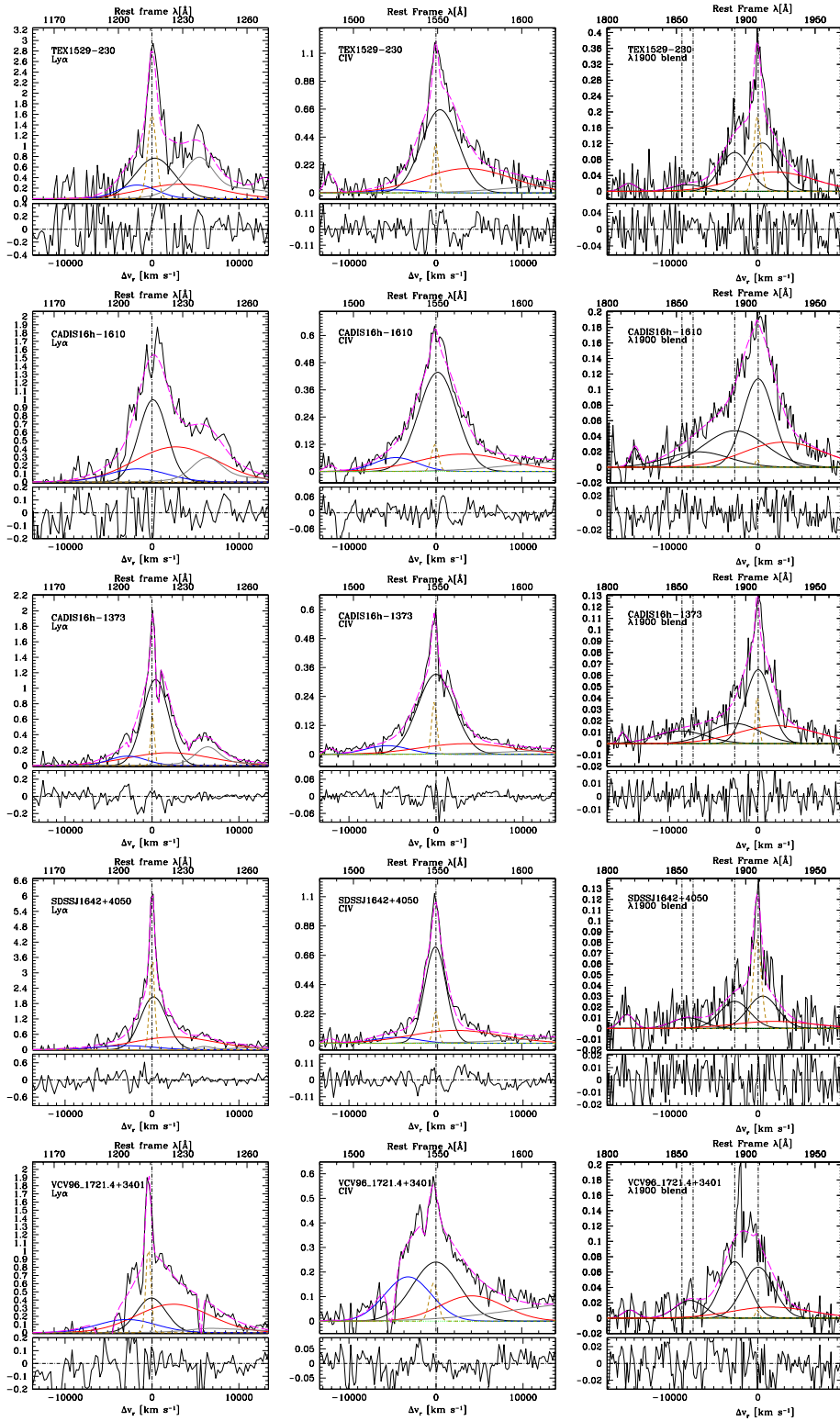


Fig. 5. (cont.)

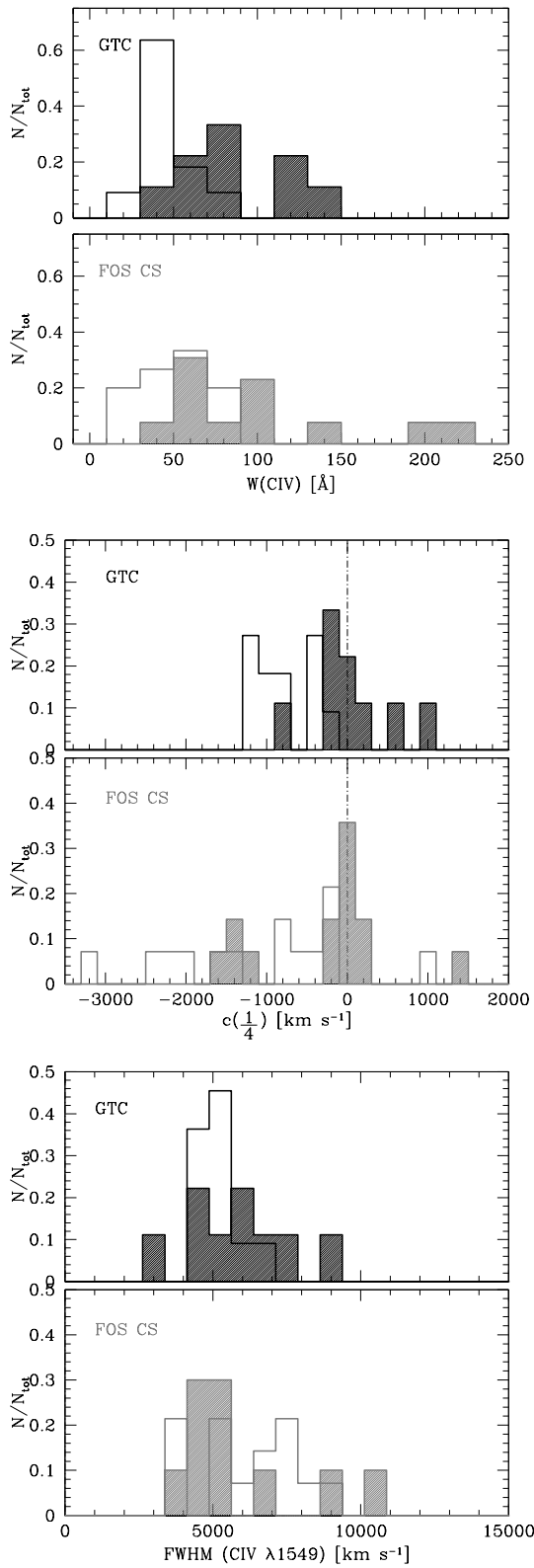


Fig. 6. Top to bottom: Distributions of $W(\text{Civ}\lambda 1549)$ for GTC (upper panel; black) and one realization of the FOS CS (grey). The shaded histogram refers to Pop. B sources. Middle: same, for the distributions of $c(\frac{1}{4})$; bottom: same for the distributions of $\text{FWHM}(\text{Civ}\lambda 1549)$.

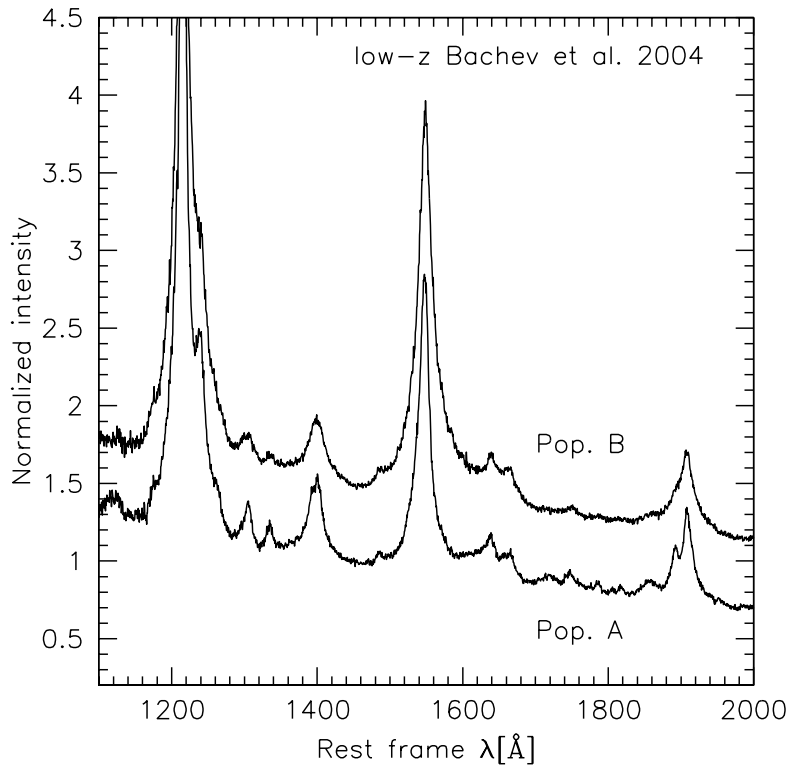
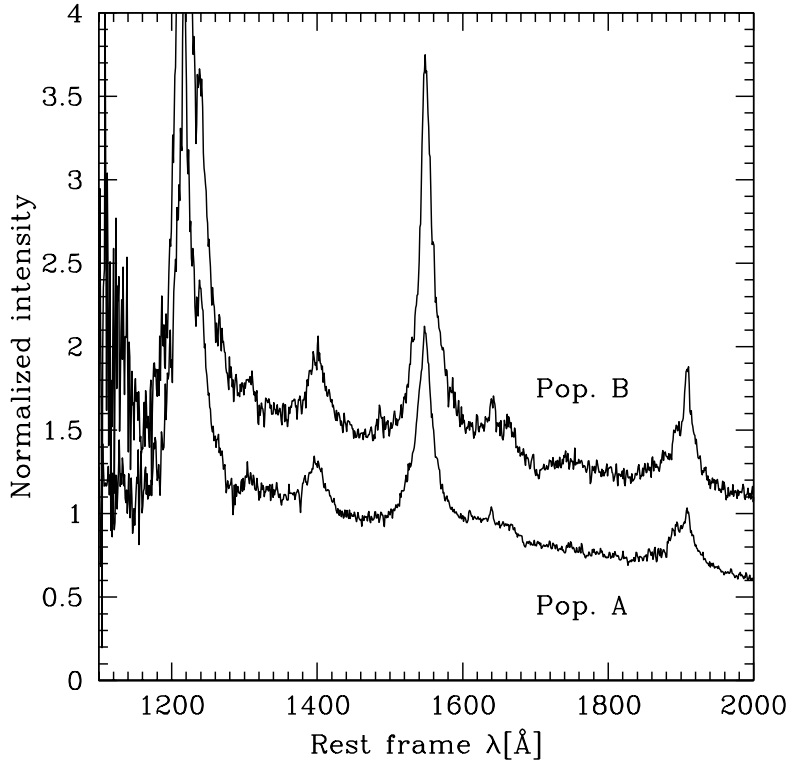


Fig. 7. Pop. A and B median spectra for the present GTC sample and for the low- z sample of Bachev et al. (2004) (bottom).

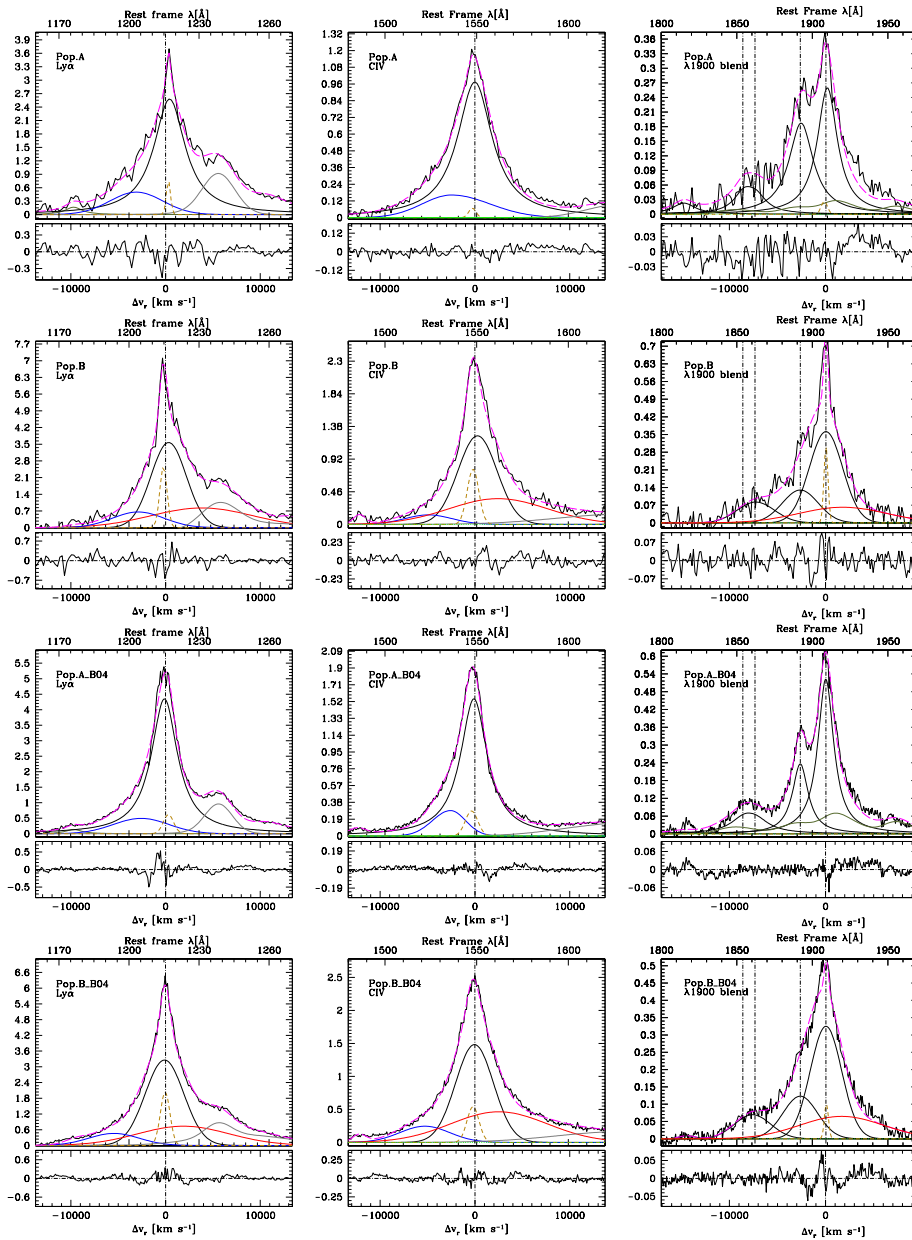


Fig. 8. Pop. A and B GTC median spectra emission line feature fits. The two lower panels show the same analysis for the Bachev et al. (2004) median composite. Meaning of colors and symbols is the same of Fig. 4 and 5.

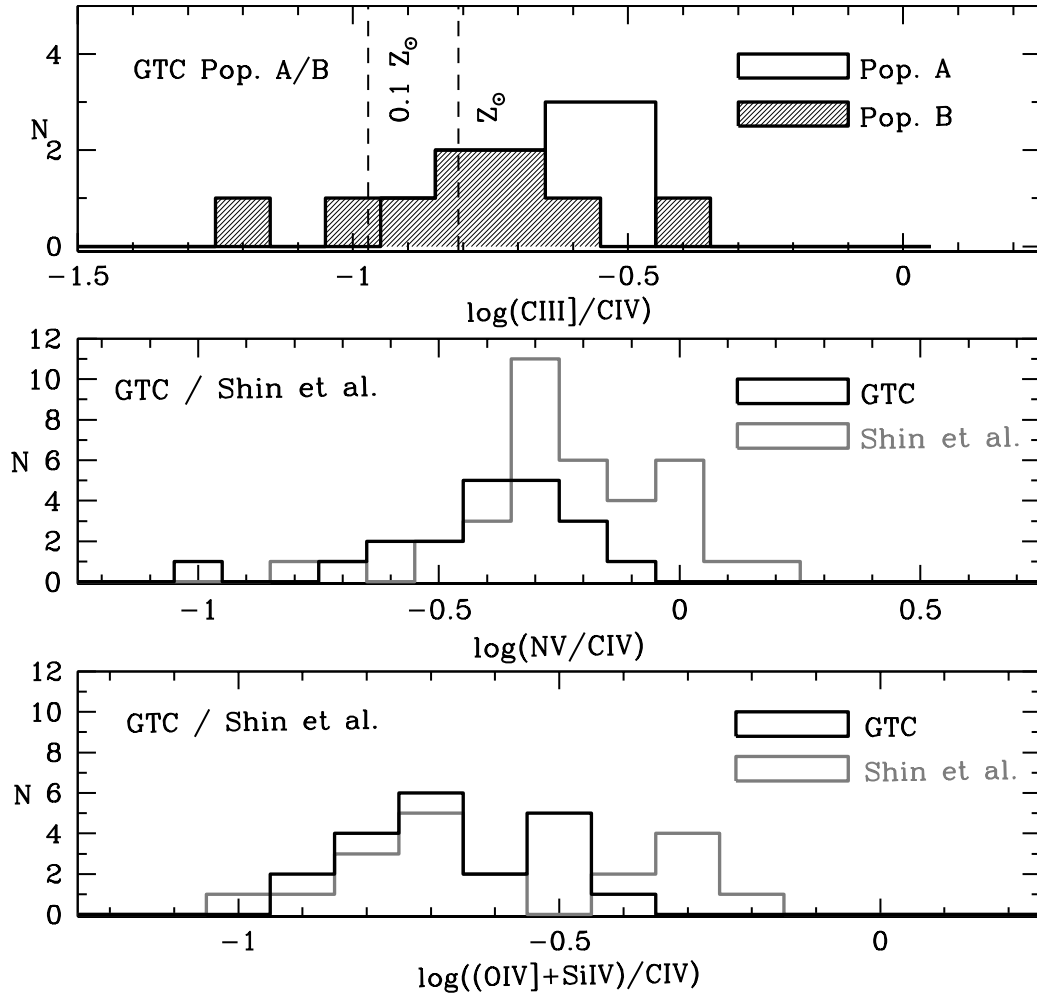


Fig. 9. Histograms showing the distributions of Z sensitive ratios. From top to bottom: $\text{CIII]}\lambda 1909/\text{CIV})\lambda 1549$ for the GTC sample (the dashed histogram is for Pop. B). Dot-dashed lines trace the expected ratios for $Z = 0.1 Z_{\odot}$ and $Z = Z_{\odot}$ for $\log n_{\text{H}} = 10$ and $\log U = -1.75$. Middle: Distribution of the ratio $\text{NV})\lambda 1240/\text{CIV})\lambda 1549$ for the GTC (black lines) and the Shin et al. (2013) low- z sample (grey lines), with the restriction $\log L \geq 46.2$ [erg s^{-1}]. Bottom: same for ratio $(\text{OIV})\lambda 1402+\text{SiIV})\lambda 1397/\text{CIV})\lambda 1549$.

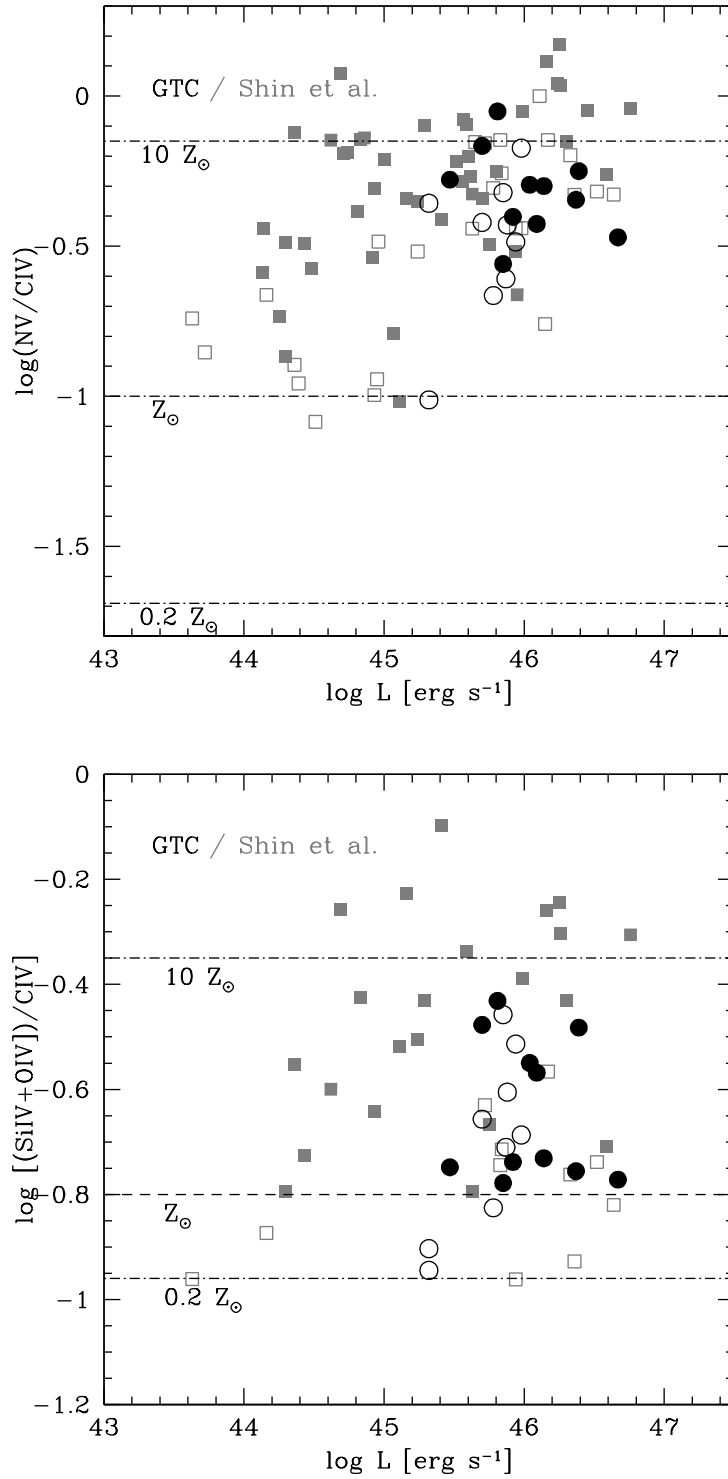


Fig. 10. Metallicity sensitive line intensity ratios as a function of bolometric luminosity for the sample of Shin et al. (2013) (grey squares) and the GTC sample (black circles). Open symbols are for Pop. B sources; filled symbols for Pop. A. Ordinate of top panel is decimal logarithm of intensity ratio between $\text{Nv}\lambda 1240$ and $\text{Civ}\lambda 1549$; ordinate of bottom panel: decimal logarithm of intensity ratio of the 1400\AA blend due to multiplets of SiIV and OIV] and $\text{Civ}\lambda 1549$. The dashed lines show the value expected for 0.2, 1, and 10 times solar metallicity following the LOC models reported in Nagao et al. (2006b).

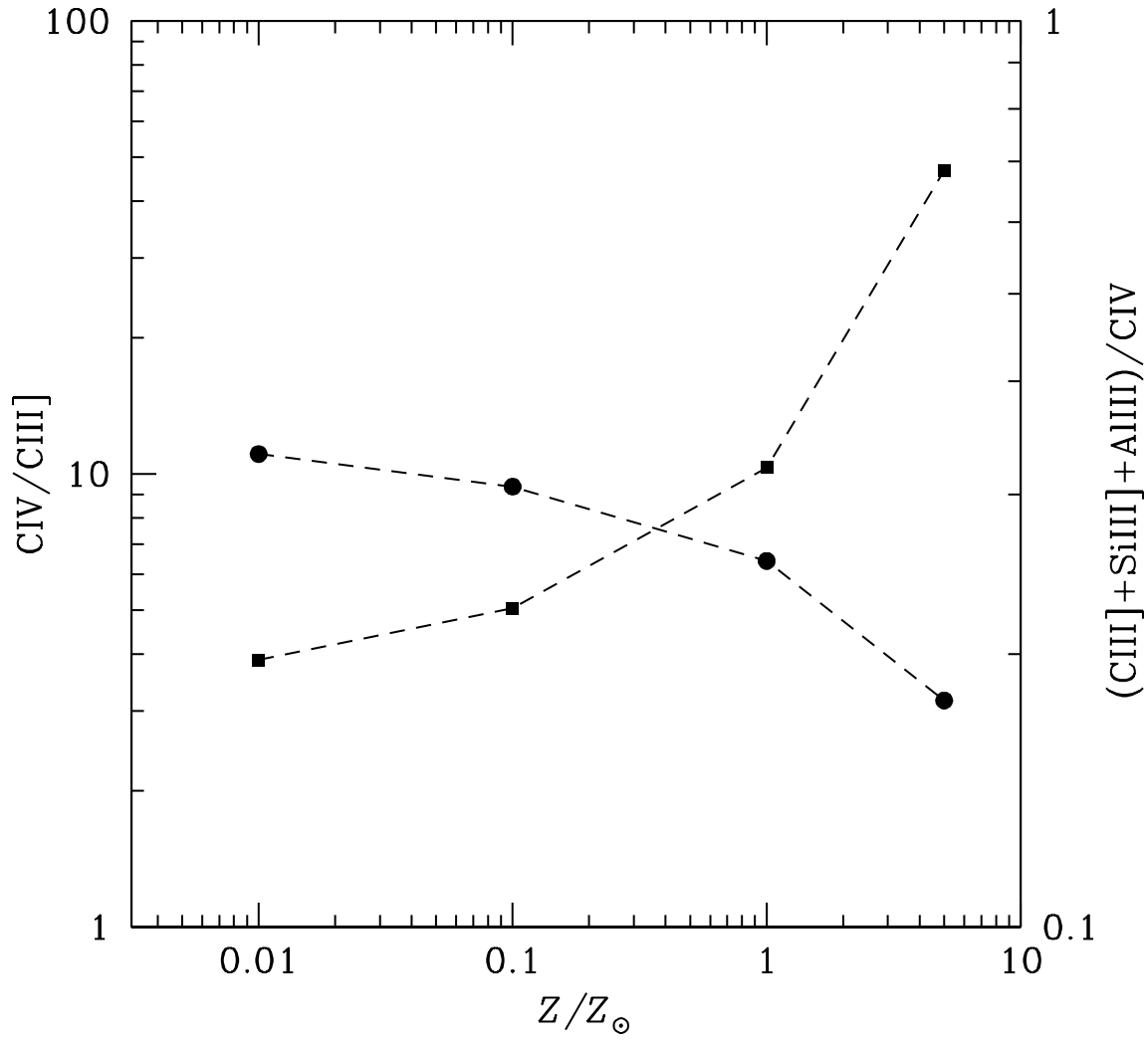


Fig. 11. Line intensity ratios $\text{CIV}\lambda 1549/\text{CIII]}\lambda 1909$ (filled circles) and total 1900 blend/ $\text{CIV}\lambda 1549$ (filled squares), for four values of Z , 0.01, 0.1, 1, 5 times solar, computed for $\log U = -1.75$ and $\log n_{\text{H}} = 10$.

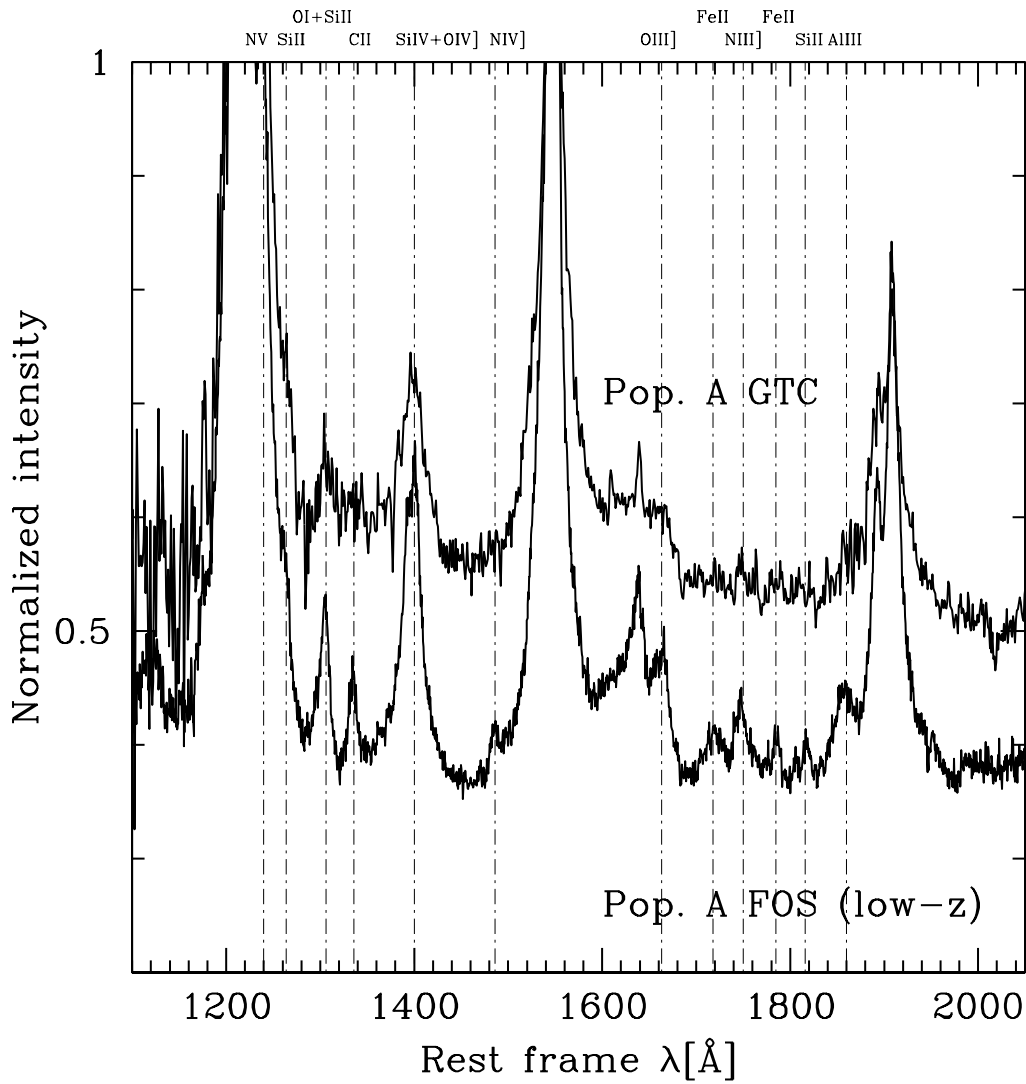


Fig. 12. Median spectra of Pop. A for the GTC sample (top) and for the spectra for the low- z sample of Bachev et al. (2004) (bottom). The continuum has been flattened and the intensity limit cut set to emphasize faint features possibly related to differences in metal content. The displacement of the two spectra is due to an artificial offset.

Appendix A: Examining a reddened quasar (tip of iceberg?) observed by GTC

Dust reddened and obscured quasars play an increasing role in the relationship between supermassive black hole growth and the evolution of galaxies on cosmic scales. Recently a new co-evolution scenario has emerged from the identification of a significant sample of red QSOs (e.g. Glikman et al. 2012, and references therein) where the reddening is not linked to the central disk/torus phenomenon but is associated with cold dust from the host galaxy that would also be experiencing starburst processes. In this scenario red-QSOs constitute a population of young high accreting quasars probably involved with a feedback mechanism. They could be precursors of the blue luminous quasars that are revealed when the dusty cocoon is swept away.

In our random selection of quasars from the Véron-Cetty & Véron (2010) catalog we included one of these red quasars. SDSS J153150.41+242317.7 (also known as FIRST 15318+2423 and F2M1531+2423) was at firstly identify as a red QSO by Glikman et al. (2007) from a sample of FIRST-2MASS candidates. They obtained NIR spectroscopy and detected broad $H\alpha$ and $H\beta$ emission lines with $z \approx 2.287$. Our GTC spectrum is shown in Figure A.1 where the highly reddened continuum is obvious as well as the presence of $Ly\alpha$, $HeII\lambda 1640$ and deep absorptions at the wavelengths of broad lines such as $CIV\lambda 1549$ and $CIII]\lambda 1909$ from which it can be classified as a mini-BAL. Taking into account all these lines we obtained a redshift of 2.284.

We have estimated the reddening of this object, parametrized by the color excess $E(B - V)$, by fitting its UV continuum with three quasar templates, excluding the regions of broad emission lines ($Ly\alpha$, $CIV\lambda 1549$, $CIII]\lambda 1909$, Fe band). In order to redden the templates we used an SMC extinction law (Gordon & Clayton 1998; Gordon et al. 2003) which appears to be the most appropriate reddening law for modeling dust reddening in quasars (York et al. 2006). We assume a R_V coefficient of 3.07 for the extinction law. Templates employed included two derived GTC composite spectra corresponding to Pop. A and B, that provide internal concordance since they were obtained from our quasar sample with the same instrumental setup, and also a third template involving the composite FIRST Bright Quasar Survey spectrum (FBQS; Brotherton et al. 2001).

The three fits yield essentially the same value for the color excess. In the first two cases, using the Pop. A & B composites, we obtained $E(B - V) = 0.41 \pm 0.01$ while the FBQS template yields $E(B - V) = 0.40$, all cases with a high correlation coefficient (≥ 0.97). Taking into account the estimated extinction, FIRST15318 becomes the brightest quasar in our sample with $M_B \approx -26.3$. In Fig. A.1 we have plotted the fitted reddened Pop A template over the observed spectrum. Attempts to learn more about its nature are difficult using the present data. Formal fitting of the red quasar continuum gives a slightly better solution as a reddened Pop A. spectrum but both Pop. A and B fits yield similar results. Taking advantage of NIR spectroscopic data (Glikman et al. 2007, 2012) allow us to model the $H\alpha$ and $H\beta$ lines. The fit for $H\alpha$ involves a Lorentzian profile with FWHM (BC) $\approx 3400 \text{ km s}^{-1}$ that identifies FIRST15318 as a Pop. A quasar in concordance with the UV continuum we fitted. In the $H\beta$ region, the spectrum is noisier but can be clearly shows the strong FeII emission characteristic of a highly accreting Pop. A sources (spectral type A2 or A3).

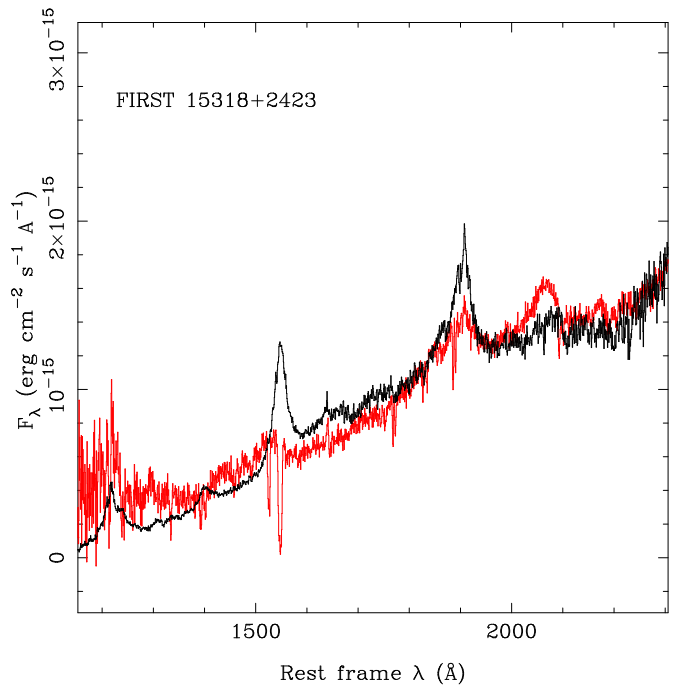


Fig. A.1. Rest frame spectrum of FIRST J15318+2423 (red). Abscissa is rest frame wavelength, ordinate rest frame specific flux. The reddened Pop. A template is shown in black. See text for more details.